

---

# Discrete Graph Auto-Encoder

**Yoann Boget**

*Geneva School for Business administration HES-SO  
University of Geneva*

*yoann.boget@hesge.ch*

**Magda Gregorova**

*Center for Artificial Intelligence and Robotics (CAIRO)  
Technische Hochschule Würzburg-Schweinfurt (THWS)*

*magda.gregorova@thws.de*

**Alexandros Kalousis**

*Geneva School for Business administration HES-SO*

*alexandros.kalousis@hesge.ch*

## Abstract

Despite advances in generative methods, accurately modeling the distribution of graphs remains a challenging task primarily because of the absence of predefined or inherent unique graph representation. Two main strategies have emerged to tackle this issue: 1) restricting the number of possible representations by sorting the nodes, or 2) using permutation-invariant/equivariant functions, specifically Graph Neural Networks (GNNs).

In this paper, we introduce a new framework named Discrete Graph Auto-Encoder (DGAE), which leverages the strengths of both strategies and mitigate their respective limitations. In essence, we propose a strategy in 2 steps. We first use a permutation-equivariant auto-encoder to convert graphs into sets of discrete latent node representations, each node being represented by a sequence of quantized vectors. In the second step, we sort the sets of discrete latent representations and learn their distribution with a specifically designed auto-regressive model based on the Transformer architecture.

Through multiple experimental evaluations, we demonstrate the competitive performances of our model in comparison to the existing state-of-the-art across various datasets. Various ablation studies support the interest of our method.

## 1 Introduction

Graph generative models are a significant research area with broad potential applications. While most existing models focus on generating molecules for *de novo* drug design, there has been interest in using these models for tasks such as material design Lu et al. (2020), protein design Ingraham et al. (2019), code programming modeling Brockschmidt et al. (2019), semantic graph modeling in natural language processing Chen et al. (2018); Klawonn & Heim (2018), or scene graph modeling in robotics Li et al. (2017).

Despite advances in generative methods, accurately modeling the distribution of graphs remains a complex task. The main challenge lies in the absence of predefined or inherent unique graph representations. Given a graph of  $n$  nodes, there are  $n!$  permutations, each corresponding to a distinct representation of the same graph.

Two main strategies have emerged to tackle this issue:

1. The first accepts multiple representations of the same graph but restricts their quantity by sorting the nodes thanks to a heuristic such as Breadth-First Search (BFS), as in You et al. (2018); Shi et al. (2020); Luo et al. (2021).

- 
2. The alternative approach employs models that are inherently invariant to node ordering permutations. This method achieves permutation invariance through the use of Graph Neural Networks, as in Vignac et al. (2023); Jo et al. (2022).

Both methods have their own challenges, which we elaborate on in Section 2.

Our main contribution is introducing a new generative model designed to address this issue of multiple graph representations. We use a permutation-equivariant auto-encoder to convert graphs into sets of node embeddings and reconstruct graphs from sets of node embeddings. Contrary to graphs, any sorting algorithm yields a unique representation for sets. So, we transform the sets into sequences and leverage an auto-regressive model to learn the implicit distribution over sets.

In implementing this framework, we introduce new methods and techniques or adapt existing ones. We enhance the node embeddings by introducing an innovative feature augmentation strategy. To ease the modeling of the latent distribution, we remove unnecessary information and reduce the size of the latent space by quantizing the node representations. However, for pragmatic considerations, we initially partition the node embeddings and subsequently quantize these partitions. As a result of this sequentialization, the latent representations form sequences spanning two dimensions: the partitions and the nodes. To model this distribution, we introduce a novel Transformer architecture designed to take advantage of its 2-dimensional structure.

The development and subsequent evaluation of our model yield several significant contributions that we summarize as follow:

- We introduce a novel generative model for graphs, leveraging a graph-to-set discrete auto-encoder invariant to permutations.
- We develop a new Transformer architecture, the 2D-Transformer, specifically designed to model sequences across two dimensions.
- We design a new technique for graph feature augmentation, which we call  $p$ -path features.
- For the first time, we empirically evaluate various feature augmentation strategies via an ablation study.
- Through empirical analysis, we show that our model outperforms existing state-of-the-art models across multiple metrics and datasets.

In the following, Section 2 presents the foundational concepts and issues of graph modeling. Section 3 discusses the literature on graph generation. In Section 4, we introduce our Discrete Graph Auto-Encoder. Lastly, Section 5 presents the experimental evaluation of our model, demonstrating its superior performance against the current state-of-the-art for various datasets, including both simple and annotated graphs.

## 2 Background

In this Section, we provide the necessary background about graph modeling. We define some notations. Then, we review the challenge of learning graph representations that mainly stem from the graph isomorphism problem. Finally, we introduce Graph Neural Networks (GNN) and discuss some of their limitations.

### 2.1 Notation

We define a simple (unannotated and undirected) graph as a tuple  $\mathcal{G} = (\mathcal{V}, \mathcal{E})$ , where  $\mathcal{V}$  is the set of nodes, whose cardinality is  $n$ , and  $\mathcal{E}$  is the set of edges between these nodes. Given two nodes  $\nu_i$  and  $\nu_j$  in  $\mathcal{V}$ , we represent the edge connecting them as  $\epsilon_{i,j} = (\nu_i, \nu_j) \in \mathcal{E}$ . For annotated graphs, we introduce two additional functions  $V$  and  $E$  that map the nodes and the edges to their respective attributes:  $V(\nu_i) = \mathbf{x}_i \in \mathbb{R}^R$  and  $E(\epsilon_{i,j}) = \mathbf{e}_{i,j} \in \mathbb{R}^S$ . In the case of univariate discrete attributes, the categorical attributes are one-hot encoded, and  $R$  and  $S$  are the number of node and edge categories, respectively. We denote an annotated graph as  $\mathcal{G} = (\mathcal{V}, \mathcal{E}, V, E)$ .

---

## 2.2 Graph isomorphism

A fundamental property of graphs is their invariance with respect to the representation ordering of the node. To put it differently, any permutation applied to the representation ordering of the node will yield an identical graph. Therefore, there are  $n!$  possible isomorphic representations of the same graph. In the following, we employ the notation  $\pi(\cdot)$  to indicate that we represent the graph under a specific node ordering.

The graph isomorphism problem, which consists of determining whether two graphs are identical or distinct, follows from these possible multiple representations Köbler et al. (1993). Algorithms that offer a unique representation for each isomorphism are at least as expensive computationally as solving the graph isomorphism problem<sup>1</sup>. This problem has not been proven to be solvable in polynomial time Helfgott et al. (2017).

As a result, algorithms that uniquely sort nodes in any graph are, at least, as expensive as algorithms solving the graph isomorphism problem.

Graph isomorphism is a significant issue for graph generative models. Without a specific solution, generative models must learn a new set of parameters for each permutation. Given the vast number of possible permutations for each graph, this brute-force approach is unreasonable. In fact, to the best of our knowledge, no generative model for graph follow such a procedure.

## 2.3 Generative models and graph isomorphism

Previous generative models, detailed in Section 3, have predominantly pursued two strategies to deal with the issue of ordering: sequentialization and invariance to permutation.

### 2.3.1 Sequentialization

The first method aims to establish an ordering of nodes that yields a sequentialization of the graph. Canonical labeling algorithms in linear time that apply to almost all graphs exist. Nevertheless, to the best of our knowledge, no generative model for graphs uses such a method. Most models adopt algorithms sorting nodes in a non-unique manner. Breadth-first search (BFS), used for instance in You et al. (2018); Shi et al. (2020); Luo et al. (2021), is the most common heuristic to order nodes in graph generative models. We presume that BFS is also a convenient way of traversing the graph and works as an inductive bias for auto-regressive models. The main drawback of BFS is that the number of potential representations can still be considerable. In the worst case (star graph), BFS does not reduce the number of possible representations at all.

### 2.3.2 Invariance to permutation

The alternative approach circumvents the issue by developing models invariant to permutation by construction. These models rely on permutation-invariant and permutation-equivariant functions. Permutation-invariance is defined as:

$$f(\mathcal{G}) = x \iff f(\pi(\mathcal{G})) = x. \quad (1)$$

A function  $f$  is said permutation-equivariant if:

$$f(\pi(\mathcal{G})) = \pi(f(\mathcal{G})). \quad (2)$$

Notably, equivariance to permutation implies that input and output have the same cardinality. In practice, Graph Neural Networks (GNN) entails permutation-invariance and permutation-equivariance. In the next Section (2.4), we introduce the fundamental principles of GNNs

---

<sup>1</sup>The graph isomorphism problem involves determining whether two graphs are isomorphic. Establishing a unique representation for each isomorphism can be considered a way to solve the problem. If the representations match, then the graphs are isomorphic.

---

## 2.4 Graph neural networks

GNN layers are permutation-equivariant functions. Since the cardinality of the input and the output of such function must match, GNNs are said to be 'flat'<sup>2</sup>.

An aggregating function providing graph-level information often follows the GNNs layers. Such an aggregation with a commutative function, as summation or averaging, results in a permutation-invariant function.

### 2.4.1 Message Passing Neural Networks

Message Passing Neural Networks (MPNNs) Scarselli et al. (2009) represent a prevalent class of Graph Neural Networks (GNNs), even though other classes of GNN have gained in popularity, in particular, GNN, where each node shares information with all the other nodes as, for instance, in Yun et al. (2019). The core concept underlying MPNNs involves updating the representation of each node by aggregating information from its neighboring nodes, those with which it shares an edge. Consequently, after  $l$  layers, each node aggregates information from its  $l$ -hop neighborhood. We refer to this  $l$ -hop neighborhood as the receptive field of node features. So, each layer increases the size of the receptive field.

**Message Passing Layer** The update of the  $l^{\text{th}}$  layer of an MPNN involves two steps. The first step computes the message:

$$\mathbf{e}_{i,j}^{l+1} = f_{\text{edge}}^l(\mathbf{x}_i^l, \mathbf{x}_j^l, \mathbf{e}_{ij}^l) \quad (3)$$

The second step aggregates information to compute a new node representation:

$$\mathbf{x}_i^{l+1} = f_{\text{node}}^l \left( \mathbf{x}_i^l, \bigoplus_{j \in \mathcal{N}(i)} \mathbf{e}_{i,j}^{l+1} \right) \quad (4)$$

In these equations, the functions  $f$  are small neural networks, the  $\bigoplus$  denotes any commutative function, and  $\mathcal{N}(i)$  is the set of nodes connected to node  $i$ . Note that the 'message'  $\mathbf{e}_{i,j}^{l+1}$  can also be interpreted as an edge representation and passed to the next layer. In the following, we will favor this interpretation.

**Limitations** MPNNs present the advantage of addressing the graph isomorphism problem, but they also exhibit some shortcomings. Specifically, two challenges have been widely acknowledged: oversmoothing and the limitation of their expressive power.

Firstly, all node and edge features tend to the same value as the number of layers increases. We call this phenomenon oversmoothing Li et al. (2018-02); Oono & Suzuki (2020). Because of it, one should limit the depth of MPNNs to a few layers.

Secondly, MPNNs exhibit limited expressive capacities in the sense that they cannot discern certain pairs of non-isomorphic graphs Morris et al. (2019). Standard MPNNs are, at best, as expressive as the Weisfeiler-Lehman (1-WL) test Xu et al. (2019); Loukas (2019). Consequently, they fail to detect some basic substructures Arvind et al. (2020); Chen et al. (2020). We illustrate such failure in Appendix D.

Two strategies to enhance the expressive capability of standard MPNNs have been proposed. Developing GNNs more powerful than MPNNs is the first strategy Maron et al. (2019); Vignac et al. (2020). So far, such GNNs are computationally much more expensive and, therefore, ineffective.

The second approach involves the augmentation of the node features with synthetic attributes, including spectral embeddings, cycle counts, and the integration of random noise. The feature augmentation enhances the ability of GNNs to capture the graph structure. Using spectral embeddings (Laplacian Positional Encoding), cycle count, or random noise is now usual as additional synthetic features for graph generation Krawczuk et al. (2021); Vignac et al. (2023). We present the details about these features in appendix D. In Section 4.1.2, we propose a new method for feature augmentation called  $p$ -path features, and in Section 5.4, we assess experimentally the effect of the various methods on our model.

---

<sup>2</sup>It does not mean that the dimension of each node representation, usually a vector, does not change.

---

### 3 Related work

In this Section, we briefly review existing work on graph generative models. As exposed in Section 2, generative models for graphs have followed two main strategies to address the graph representation issue: sequentialization and invariance to permutation.

#### 3.1 Sequential generation

This sequentialization serves dual purposes: it restricts the number of possible graph representations and facilitates auto-regressive graph generation. Notably, all models following this approach are auto-regressive. Graph canonization is computationally expensive, as discussed in Section 2. To the best of our knowledge, GraphGen Goyal et al. (2020) stands as the only model employing this particular strategy for generic graphs. Most works only seek to reduce the number of graph representations by adopting a Breadth-First Search (BFS) based method.

We can further categorize auto-regressive models into two classes. The first class, which includes the seminal GraphRNN You et al. (2018), employs a recurrent framework that necessitates maintaining and updating a global graph-level hidden state. This approach inherently introduces long-range dependencies, as proximate nodes in graph topology can be distant in the sequential representation. The second class of auto-regressive models sidesteps long-range dependencies by recomputing the state for the partially generated graph at each step Shi et al. (2020); Luo et al. (2021); Liao et al. (2019); Kong et al. (2023). Although this alleviates the long-range dependency issues, it drastically increases the computational cost.

Furthermore, auto-regressive models, generating nodes and edges one by one, are inherently slow during the generation phase. Generation slowness is especially true for the second class of models, as highlighted by experimental results in Section 5.3.2 and in Jo et al. (2022). GRANs Liao et al. (2019) attempt to address this speed issue by generating multiple nodes and edges simultaneously, albeit with a trade-off in generation performance.

Models previously discussed are generic, meaning they operate independently of any specific domain knowledge. However, many models are tailored to particular domains, notably in the domain of molecule generation, which represents a predominant application of graph generative modeling. Such domain-specific models often employ canonical representations. The Canonical SMILES notation, for instance, is commonly used to represent molecules, as in Gómez-Bombarelli et al. (2018); Kusner et al. (2017). Recently, powerful models representing molecules as 3d objects have emerged Hoogeboom et al. (2022); Xu et al. (2023). While plenty of domain-specific sequential models exist Liu et al. (2018); Samanta et al. (2020); Jin et al. (2018; 2020); Kuznetsov & Polykovskiy (2021); Li et al. (2018), in this work, we focus on developing a generic graph model.

#### 3.2 Models invariant to permutations

The second main strategy to address the multiple potential representations of a graph consists of using models invariant to permutations. By definition, these models, also referred to as 'one-shot', cannot be sequential. These models implement invariance or equivariance through GNNs. They are thus insensitive to the ordering of the graphs during training. Various methods, such as Generative Adversarial Networks (GANs), Normalizing Flows (NF), and diffusion/score-base models, have been proposed following this strategy, each with its merits and issues.

In GANs, a discriminator (or critic) classifies (or scores) graphs between true (from the dataset) and generated, while a generator aims to maximize the error of the discriminator. MolGAN De Cao & Kipf (2018) proposes to use permutation-invariant discriminator. GG-GAN Krawczuk et al. (2021) add a permutation-equivariant generator, and GrannGan Boget et al. (2023) proposes to generate only the nodes and edges attribute from sampled skeletons. However, the adversarial training is known to be unstable. MolGAN exhibits mode collapse and low diversity. GG-GAN also suffers of lack of diversity, while GrannGAN does not generate graphs, but only their attributes.

Normalizing Flows are designed to learn an invertible mapping between the data distribution and a known continuous distribution, typically the Standard Normal distribution. Both GraphNVP Madhawa et al. (2019)

---

and Moflow Zang & Wang (2020) use a two-step process, first generating an adjacency tensor, followed by an annotation matrix conditioned on this tensor. GNF Liu et al. (2019) needs only one step but focuses on generating simple graphs only.

However, we hypothesize that, even with dequantization, efficiently spanning the continuous latent space using discrete objects remains a significant challenge. Indeed, based on their empirical evaluations, while these models surpass the performance of GAN-based approaches, they do not model graph distributions as effectively as auto-regressive models and those relying on diffusion/score-based methods.

Diffusion and score-based models gradually introduce Gaussian noise to the data and learn to denoise it for each noise level. In graphs, some models have suggested adding Gaussian noise to the adjacency matrix Yang et al. (2019) and to the annotation matrix Jo et al. (2022). By doing so, these models generate fully connected graphs, facilitating direct information sharing among all nodes. Such an approach effectively captures the global structure of the graph and, as of now, has produced the best results, with GDSS Jo et al. (2022) considered as state-of-the-art.

However, as stated in Vignac et al. (2023), the continuous noise compromises the graph structures, leading them to collapse into fully connected graphs. To address this concern, DiGress introduced a discrete diffusion model for graphs Vignac et al. (2023), which integrates discrete noise to maintain a coherent graph structure at every noise level. In practice, however, the discretization does not appear to bring significant improvement over GDSS. Whether continuous or discrete, the extensive denoising steps integral to score-based/diffusion models make the generation process comparatively slow, as shown experimentally and reported in Section 5).

### 3.3 Graph Auto-Encoders

Closer to our work, Kipf and Welling Kipf & Welling (2016) proposed a permutation-equivariant graph auto-encoders, namely the Graph Auto-Encoder (GAE) and the Variational Graph Auto-Encoder (VGAE) relatively long ago. However, they use it as a feature extractor for downstream tasks rather than for generation. In fact, neither of these two models captures the interaction and dependencies between node embeddings. One of our main contributions consists of modeling these interactions and dependencies necessary for generation. On a side note, we also remark that they use a simple activated scalar product as a decoder, which can neither capture interactions between multiple node embeddings nor decode node and edge attributes. Like most auto-encoders in generative modeling, we use a decoder mirroring the encoder.

Lastly, GraphVAE Simonovsky & Komodakis (2018) adopts a distinct approach to handle the multiple possible graph representations. A permutation-invariant encoder captures a graph-level latent representation, losing the original node ordering in their aggregation. Then, a decoder, built using a standard feed-forward neural network, aims to reconstruct the original graph to yield a graph in any permutation. Nevertheless, during the training phase, the model requires aligning the original representation with its reconstructed counterpart. This comparison necessitates an expensive graph-matching procedure with a computational complexity of order  $\mathcal{O}(n^4)$ .

Unlike GraphVAE, our auto-encoder is permutation-equivariant end-to-end. Its goal is not to capture the graph-level representation but a set of node embeddings, each capturing its local neighborhood so that we can reconstruct the graph from its set of node embeddings. Since the sequentialization of sets does not suffer the same problem as graphs, we can model the set of node embeddings as a sequence leveraging an auto-regressive model. To sum up, we follow the permutation invariance strategy to train a graph-to-set auto-encoder, and then we follow the sequentialization strategy to model the distribution over sets.

## 4 Discrete Graph To Set Auto-Encoder

In a nutshell, our approach involves a two-step strategy. The first step is a graph auto-encoder. We encode a graph into a set of  $n$  node embeddings. For practical reasons detailed hereunder, we partition each node embedding into  $C$  vectors and quantize each vector independently. Then, we decode the quantized latent

representation, aiming to recover the original graph. This first step generates a discrete latent distribution over sets of node embeddings, yet this latent distribution remains unknown.

In the second step, our objective is to learn this latent distribution. Rather than directly modeling a distribution over sets, we transform the sets into sequences. We then leverage a model based on the Transformer architecture to learn these sequences auto-regressively.

The rationale behind this two-step strategy stems from using permutation-equivariant functions, particularly Message Passing Neural Networks (MPNNs), to project the graph into a latent space and decode it. This approach prevents the node ordering issue, making the computation of the reconstruction loss straightforward without needing a matching procedure. However, as discussed in Section 2.4.1, MPNNs present inherent limitations, such as being constrained in depth and only capturing information from their  $L$ -hop neighborhood,  $L$  being the number of layers in the MPNN. Consequently, MPNNs are unable to model interactions between distant nodes. Therefore, we introduce the second step to model the latent distribution to address these long-range dependencies between node embeddings.

In this Section, we present and motivate these two steps in detail (Sections 4.1 and 4.2), and we explicitly explain how we perform generation (Section 4.3).

### 4.1 Discrete Graph Auto-Encoder

In this initial step, our primary objectives when encoding graphs are twofold. Firstly, we aim to learn node embeddings that facilitate the accurate reconstruction of the original graph. Secondly, we strive to create a latent distribution that is handy to learn in the second step.

To achieve this, we enhance the input graph representation with feature augmentation (Section 4.1.1). We use a Message Passing Neural Network (MPNN) to encode graphs  $\mathcal{G}$  into sets of node embeddings  $\{z_1^h, \dots, z_n^h\} = \mathcal{Z}^h$ , mapping a space over graphs to a space over sets  $f_{encoder} : \mathbb{G} \mapsto \mathcal{Z}^h$  (Section 4.1.2). Partitioning and quantizing the node embeddings results in a handy discrete latent space with known support, facilitating the modeling of the latent distribution in the second step. Specifically, we partition the node embeddings in a sequence of  $C$  vectors  $z_i^h = (z_1^h, \dots, z_C^h)$ . We then quantize each vector independently (Section 4.1.3), replacing them with their closest neighbor in a codebook. Finally, another MPNN decodes the sets of quantized vectors  $\mathcal{Z}^q$ , also called codewords, to graphs  $\hat{\mathcal{G}}$ , formally  $f_{decoder} : \mathcal{Z}^q \mapsto \mathbb{G}$ . Figure 1 visually summarizes the entire procedure.

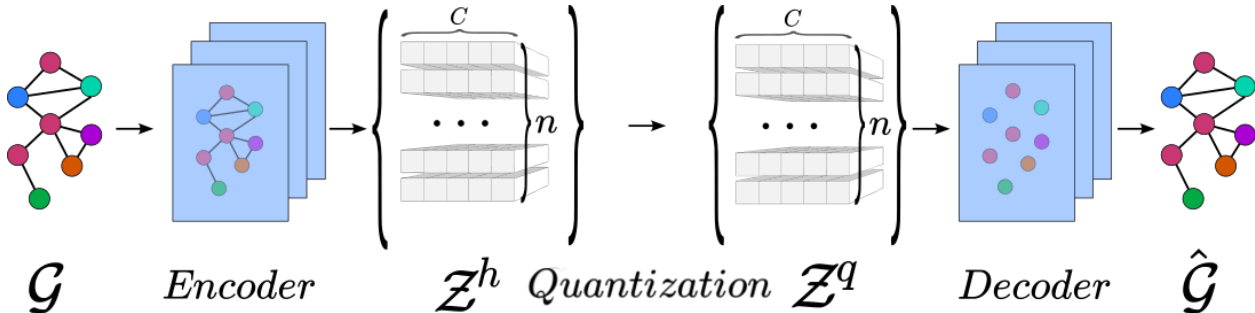


Figure 1: Diagram of our auto-encoder. 1. The encoder is an MPNN transforming the graph into a set of node embeddings  $\mathcal{Z}^h$ . 2. The elements of the set  $\mathcal{Z}^h$  are partitioned and quantized, producing a set of codeword sequences  $\mathcal{Z}^q$ . 3. The decoder, an other MPNN, takes the set  $\mathcal{Z}^q$  and reconstruct the original graph.

#### 4.1.1 Input Graph and Feature Augmentation

As explained in Section 2.4, conventional MPNNs cannot identify certain fundamental graph substructures. Such a shortcoming adversely impacts the information captured by the encoder. Inevitably, the node embeddings miss the information the encoder fails to capture, preventing accurate reconstruction. A common mitigation strategy involves enhancing MPNN capacities by augmenting the input features with synthetic

attributes. We employ this approach to generate more informative node embeddings, allowing for better reconstruction performance.

Here, we propose a new augmentation scheme that aggregates information from the  $p$ -path neighborhood. Specifically, we first create virtual edges (with a vector of zeros as attributes) between nodes that are connected by paths of length 2 to  $p$  (the edges between adjacent nodes, i.e. connected by a path of length 1, are already represented by a vector of edge attributes). We then concatenate a synthetic  $p$ -dimensional vector to each vector of edge attribute, whose  $i^{th}$  entry corresponds to the number of paths of length  $i$  connecting the two endpoints. Similarly, we augment the node features with a  $p$ -dimensional vector, whose  $i^{th}$  entry indicates the number of paths of length  $i$  emanating from the node. In Appendix D, we provide more details on how we compute the path lengths as well as information about the other feature augmentation schemes used for our experiments.

Our method presents two benefits compared to other methods. First, unlike other methods, our  $p$ -path augmentation strategy produces synthetic attributes for nodes *and* edges, providing richer information about the substructures around each node. Second, the virtual edges aggregate information from a larger neighborhood. The computation of the synthetic features is a unique preprocessing step. In our experiments, we use the  $p$ -path method setting  $p = 3$ .

Our solution is related to the recent  $k$ -hop message passing presented in Feng et al. (2022), both using the path length information. Our proposition differs on two main points. First, we use the path information to create synthetic features, while  $k$ -hop message passing uses this information to compute different message passing functions for each path length. Second, we take into account the number of paths of length  $p$  between 2 nodes, while they only consider if there is at least one such path.

In Section 5.4, we empirically show that our method increases the reconstruction performance of our auto-encoder the most compared to other methods.

#### 4.1.2 Encoder

We aim to encode graphs as sets of node embeddings, where each embedding captures its local graph structure so that we can effectively recover the original graph from these embeddings. We use an MPNN as encoder since they are specifically designed and efficient for modeling the local neighborhood of each node.

We formally define our encoder as an  $L$ -layer MPNN whose layers follow these two equations:

$$\mathbf{e}_{i,j}^{l+1} = \text{bn}(f_{\text{edge}}([\mathbf{x}_i^l, \mathbf{x}_j^l, \mathbf{e}_{i,j}^l])) \quad (5)$$

$$\mathbf{x}_i^{l+1} = \text{bn} \left( \mathbf{x}_i^l + \sum_{j \in \mathcal{N}(i)} f_{\text{node}}([\mathbf{x}_i^l, \mathbf{x}_j^l, \mathbf{e}_{i,j}^l]) \right), \quad (6)$$

where  $\text{bn}$  stands for *batch normalization* Ioffe & Szegedy (2015) and  $[\cdot, \cdot]$  is the concatenation operator. After the last layer, we discard the edge representation  $\mathbf{e}_{i,j}^L$  and keep only the node representation so that  $\mathbf{z}_i^h = \mathbf{x}_i^L \in \mathbb{R}^{d_{\text{latent}}}$ . The complete graph latent representation is the set of all the node embedding  $\mathcal{Z}^h = \{\mathbf{z}_1^h, \dots, \mathbf{z}_n^h\}$  where the superscript  $h$  indicates the set before quantization. The superscript  $q$  will refer to the latent representations after quantization.

#### 4.1.3 Discrete Latent Distributions

In the context of our auto-encoder, quantization consists of replacing a  $d$  dimensional vector by its nearest neighbor in a learned codebook  $H \in \mathbb{R}^{m \times d}$ ,  $m$  being the codebook size. By partitioning, we refer to a simple reshaping operation, where a vector of dimension  $d$  is reshaped in  $C$  vector of dimension  $d/C$ . Both operations follow the same objectives: produce a latent distribution that is handy to model (in the second step) and flexible enough to yield good reconstruction.



Specifically, the encoder outputs  $n$  node embeddings  $\mathbf{z}_i^h \in \mathbb{R}^{d_{latent}}$ . So, we partition these node embeddings in  $C$  vectors  $(\mathbf{z}_{i,1}^h, \dots, \mathbf{z}_{i,C}^h)$ , where each  $\mathbf{z}_{i,c}^h$  is in  $\mathbb{R}^{d_{latent}/C}$ . Then, we quantize each vector independently. We refer to the partitioned and quantized representations as the discrete latent representation  $\mathcal{Z}^q = \{(\mathbf{z}_{1,1}^q, \dots, \mathbf{z}_{1,C}^q), \dots, (\mathbf{z}_{n,1}^q, \dots, \mathbf{z}_{n,C}^q)\}$ . Figure 2 depicts the quantization procedure. Partitioning and quantization result in discrete latent distributions.

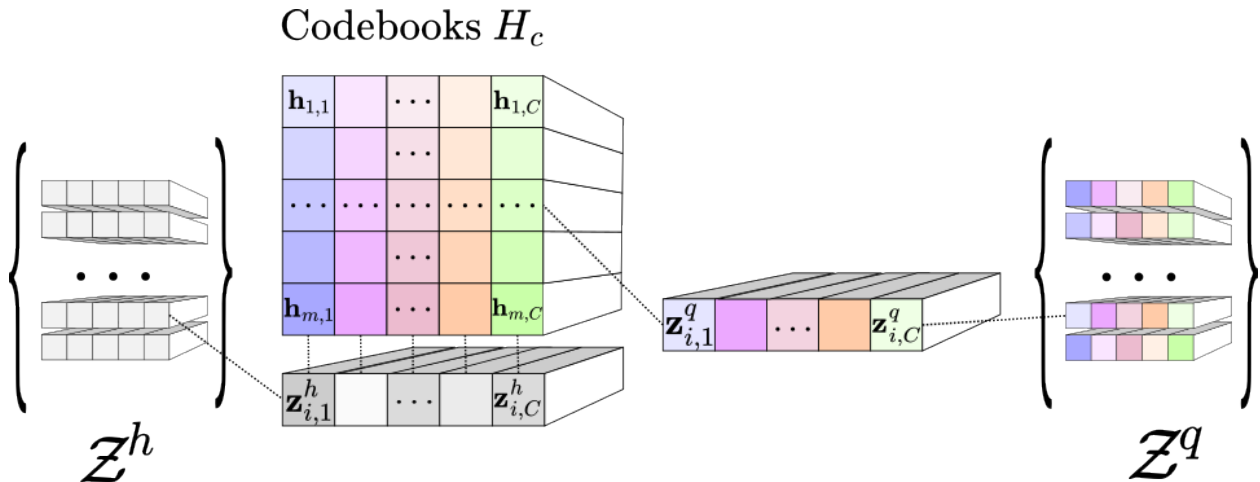


Figure 2: Diagram of the quantization. We represent each node embedding by  $C$  partition vectors  $\mathbf{z}_{i,c}^h$ . Then, we quantize each of these vectors by replacing them with their closest neighbor from the corresponding codebook  $H_c$ . The vectors in the codebooks are parameters learned during training.

**Discrete Latent Representations** The node embeddings  $\mathbf{z}_i^h$ , as they are output by the encoder, are real-valued vectors in  $\mathbb{R}^{d_{latent}}$ . We make two observations regarding these vectors.

First, if the original graphs have only discrete node and edge attributes, the support of this distribution is discrete. It corresponds to all the possible subgraphs within the  $L$ -hop neighborhood, where  $L$  is the number of encoder layers. However, enumerating the support of this discrete distribution is intractable in almost all practical scenarios, which makes the modeling of this discrete distribution unpractical. In the continuous case, the distribution of the node embeddings remains also unknown and challenging to model.

Second, the encoder cannot model interactions between distant nodes. By consequence, even if we could model the distribution of each node embedding individually, the distribution over the sets of node embeddings would remain unknown.

Both observations, i.e., the potential discrete support of the node embedding distributions and the impossible modeling of distant nodes, make standard variational auto-encoder unappropriated for the task. More generally, the distribution of node embeddings  $\mathbf{z}_i^h$ , as they are output by the encoder, is challenging. On the other hand, discrete latent models have shown impressive results with both discrete and continuous data van den Oord et al. (2017); Razavi et al. (2019). Therefore, we leverage such a model using quantization to produce discrete latent distributions with known support.

**Quantization** The quantization of the node embeddings into discrete latent representations presents many advantages. First, discrete latent representation is a natural fit for modeling discrete structures like graphs. In particular, discrete representation prevents approximating step functions or Dirac delta functions with neural networks, which require smooth differentiable functions.

Quantization also enforces the codewords to follow a  $m$ -dimensional categorical distribution, where  $m$ , the codebook size, is a hyper-parameter. Knowing that the latent vectors follow an  $m$ -dimensional categorical distribution, we can learn their parameters in the second stage of our model.

Moreover, quantization acts as an information bottleneck. Assuming no prior information, the information contained in each selected codeword is  $I = \log_2(m)$  bits and depends only on the codebook size  $m$ . By

training the auto-encoder with a reconstruction objective, we encourage the quantization process to retain only the most valuable information for reconstruction. Also, by reducing the codebook size, we shrink the number of categories and, therefore, the number of parameters of the categorical distribution, making the latent distribution easier to learn. Limiting the codebook size also reduces the risk of codebook collapse Kaiser et al. (2018) as observed in our experiments (See Section 5.4), favoring a better coverage of the space and so preventing sampling from regions out of the distribution. However, restraining the information passed to the decoder makes the reconstruction harder. As a result, there is a trade-off between the reconstruction quality and the dimensionality of the categorical distribution stemming from the codebook size. We empirically show the effect of this trade-off in our experiments (See Section 5.4). We indeed observe that the reconstruction loss decreases when the codebook size increases. However, larger codebook sizes do not yield better generation performances despite better reconstruction performance. We explain this observation because larger codebooks result in larger categorical distributions that are harder to learn.

**Partitioning** In practice, we often need a large discrete latent space to model each node representation with enough flexibility. We can obtain this flexibility either with a single codeword with a large codebook or with multiple codewords, each coming from a (much) smaller codebook.

Large codebooks imply high dimensional categorical distributions, which are inconvenient in practice. Specifically, modeling a high-dimensional categorical distribution in the second stage of our model would require an output layer whose size corresponds to the dimension of this distribution. Large output layers, particularly those larger than their hidden layers, are ineffective in practice. Our experiments show that our model’s generation performance drops for the larger categorical distribution.

So, instead of representing each node embedding with a single codeword, we use multiple codewords for each node representation. To that end, we partition the node embeddings  $\mathbf{z}_i^h \in \mathbb{R}^{d_{latent}}$  in  $C$  vectors  $\mathbf{z}_{i,c}^h, c \in \mathbb{R}^{d_{latent}/C}$  by reshaping them.

$C$  vectors, therefore, represent each node embedding, each being quantized independently of each partition with its own codebook. In fact, in graphs, as in images, codebooks shared across features reflect an invariance assumption: the permutation invariance for graphs and the translation invariance for images. We use different codebooks for the different partitions as we do not assume any invariance across partitions. In other words, there is no reason to share codebooks across partitions because the various partitions do not belong to the same feature map.

After partitioning and quantization, the latent representation of each node is a sequence of codewords. We call dictionary the set all possible codeword arrangements. Therefore, for a fixed codebook size  $m$ , the dictionary size is  $M = m^C$ . We empirically assess the effect of partitioning and present the results in Section 5.4.

**Formalisation** Specifically, the partition function  $f_p$  defines a simple reshaping operation transforming a vector of dimension  $d_{latent}$  in  $C$  vectors of dimensions  $d_{latent}/C$ , that is  $f_p : \mathbb{R}^{d_{latent}} \mapsto \mathbb{R}^{C \times (d_{latent}/C)}$ .

We define the quantization function  $q_c : \mathbb{R}^{d_{latent}/C} \mapsto \{\mathbf{h}_{1,c}, \dots, \mathbf{h}_{m,c}\}$  as the mapping of the  $c$ -th partition of node  $i$ , to its closest neighbor in the corresponding codebooks  $H_c \in \mathbb{R}^{m \times d_{latent}/C}$ , such that:

$$q_c(\mathbf{z}_{i,c}^h) = \mathbf{z}_{i,c}^q = \mathbf{h}_{k,c} \quad \text{with} \quad k = \arg \min_g (||\mathbf{z}_{i,c}^h - \mathbf{h}_{g,c}||_2). \quad (7)$$

Notably, the quantization procedure acts independently on every element in the set. It is, therefore, permutation-equivariant.

We underline that a bijection exists between the quantized vectors and their corresponding indices in the codebooks. Therefore, the quantized vectors and their indices hold the same information. In the following, we refer to the set of indices corresponding to the set of quantized vectors as  $\mathcal{Z}^q = \{(\mathbf{z}_{1,1}^q, \dots, \mathbf{z}_{1,C}^q), \dots, (\mathbf{z}_{n,1}^q, \dots, \mathbf{z}_{n,C}^q)\}$  as  $\mathcal{K} = \{(k_{1,1}, \dots, k_{1,C}), \dots, (k_{n,1}, \dots, k_{n,C})\}$ , where  $k_{i,c} \in \{1, \dots, m\}$ .

---

#### 4.1.4 Decoder

After quantization, the decoder has to recover the graph structure and the node and edge attributes for annotated graphs. Formally, it is a set-to-graph function  $f_{decoder} : \mathbb{Z}^q \mapsto \mathbb{G}$ . Since we have dropped any explicit representation of the graph (see Section 4.1.2), when we decode it, we assume a fully connected graph among the elements of  $\mathbb{Z}^q$ . We subsequently feed the fully connected graph into an MPNN similar to the one used as encoder but without feature augmentation. The decoder output serves as logit to model the discrete distributions over the edges and the nodes when the graph has node attributes. We present the implementation details in Appendix A.1.

#### 4.1.5 Training

Our training strategy follows principles developed to train models performing quantization of the latent space van den Oord et al. (2017). The training objectives are simultaneously reconstruction and quantization. We define a reconstruction loss for the first objective. We update the codebook vectors center using Exponential Moving Average (EMA) as second objective. Lastly, we add a regularization term to prevent the latent space from growing indefinitely. In the following, we present these elements and provide the implementation details in Appendix A.2.

**Reconstruction loss** We train the parameters of MPNNs (encoder and decoder) to minimize the reconstruction loss. We define it as the expected negative log-likelihood of the graph given the set of codewords  $\mathbb{Z}^q$ :

$$\mathcal{L}_{recon.} = -\mathbb{E}_{\mathbb{Z}^q} \ln(p_{\theta}(G|\mathbb{Z}^q)) \quad (8)$$

Thanks to the auto-encoder’s permutation-equivariance, the loss computation is straightforward since the representation order of the output corresponds to the input one.

The main difficulty comes from the quantization operation, which is non-differentiable. Therefore, no gradient can flow back to the encoder. We circumvent this difficulty by following van den Oord et al. (2017) and passing the gradient with respect to the codeword directly to the encoder’s output, bypassing the quantization operation.

**Vector Quantization Objective** The Vector Quantization (VQ) objective updates the vector in the codebooks. The objective function, acting as an online  $k$ -means algorithm, updates the vectors in the codebook using EMA as proposed in van den Oord et al. (2017). We adopt the  $k$ -mean++ initialization for the codebooks as proposed in Łańcucki et al. (2020).

**Commitment loss** Finally, nothing prevents the embeddings from taking arbitrarily large values. To circumvent this issue, we follow again van den Oord et al. (2017). We incorporate a commitment loss function, which pushes the encoder outputs close to their corresponding codewords. .

## 4.2 Modeling The Latent Distribution

The auto-encoder implicitly defines a distribution over the latent space  $\mathbb{Z}^q$ , which translates over the space of the corresponding sets of indices  $\mathbb{K}$  defined in Section 4.1.3. For generation, we need to sample from one of these distributions. So, we decide to model the distribution of indices. After sampling, we recover the corresponding codewords from their indices.

Instead of learning a distribution over the sets of index partitions  $\{(k_{1,1}, \dots, k_{1,C}), \dots, (k_{n,1}, \dots, k_{n,C})\}$ , we turn the sets into sequences by sorting them. After sorting, the sequences of indices  $\mathbb{K} \in \mathbb{R}^{n \times C}$  have two dimensions: the partition dimension and the node dimension. Instead of flattening the sequence, we propose a new model based on the Transformer architecture Vaswani et al. (2017) that leverages the 2-dimensional structure of the sequences to implement parameter sharing for computational efficiency and better generalization. We call it 2D-Transformer.

Our main contribution concerns the attention function. Before presenting it, we first detail the sequentialization, the auto-regressive process, the input and output of our model, and recall some basics of the Transformer architecture.

### 4.2.1 Sequentialization

The existence of multiple permutations carries over from the graphs to the sets in the latent space. The multiple possible representations are still an issue, as well as the limitations of permutation-equivariant and permutation-invariant functions are still an issue.

However, unlike graphs, sorting sets in a unique representation is easy. Any sorting algorithm can sort sets, yielding a unique representation. We can then represent the latent distributions as sequences and learn them auto-regressively.

Additionally, we remark that sorting is a specific kind of permutation. Since the decoder is permutation-equivariant, permuting the node embeddings in the latent space only changes the representation of the output graph but not the graph itself. So, we sequentialize the sets and learn the sequential distribution auto-regressively.

the set of quantized vectors as  $\mathcal{Z}^q = \{(\mathbf{z}_{1,1}^q, \dots, \mathbf{z}_{1,C}^q), \dots, (\mathbf{z}_{n,1}^q, \dots, \mathbf{z}_{n,C}^q)\}$  as  $\mathcal{K} = \{(k_{1,1}, \dots, k_{1,C}), \dots, (k_{n,1}, \dots, k_{n,C})\}$ , where  $k_{i,c} \in \{1, \dots, m\}$ . In practice, we sort the set of index sequences  $\mathcal{K} = \{(k_{1,1}, \dots, k_{1,C}), \dots, (k_{n,1}, \dots, k_{n,C})\}$  (the indices corresponding to the codewords  $\mathcal{Z}^q = \{(\mathbf{z}_{1,1}^q, \dots, \mathbf{z}_{1,C}^q), \dots, (\mathbf{z}_{n,1}^q, \dots, \mathbf{z}_{n,C}^q)\}$ , see Section 4.1.3) by increasing order using the first partition as the primary criterion. In case of a tie, we use the index of the second partition as a secondary criterion, etc. We permute the set  $\mathcal{Z}$  accordingly. We obtain sequences of indices  $K \in \mathbb{R}^{n \times C}$  and, the corresponding sequence of codewords  $Z \in \mathbb{R}^{n \times C \times d_{latent}/C}$ .

Since we perform the sorting operation as a preprocessing step for second stage of our model, there is no backpropagation through the sorting operation.

The ordering obtained is arbitrary, but it has the advantage of being completely generic. Domain-specific information can certainly lead to orderings that improve learning performance. We let this question open for further domain-specific research.

In terms of notation, we remove the superscript  $q$  from the latent vector  $\mathbf{z}$  since we only work with the selected codewords in this second stage. Instead, we use the superscript to indicate the number of Transformer blocks traversed so that  $\mathbf{z}_{i,c}^l$  correspond to the representation  $\mathbf{z}_{i,c}$  after  $l$  blocks.

### 4.2.2 Auto-regressive setup on two dimensions

Our model uses the codewords vectors  $Z$  as input to model the distribution of indices  $K$ . Formally, we have:

$$P((k_{1,1}, \dots, k_{1,C}), \dots, (k_{n,1}, \dots, k_{n,C})) = \prod_{i=1}^n \prod_{c=1}^C P(k_{i,c} | \mathbf{z}_{<i,1}, \dots, \mathbf{z}_{<i,C}, \mathbf{z}_{i,<c}), \quad (9)$$

where  $\mathbf{z}_{<i,j}$  refers to all the vectors having the first index smaller than  $i$  and  $j$  as second index.

We introduce the description of the inputs and outputs of our model as it should help to understand how our auto-regressive model access to all and only allowed positions.

For the input, we offset the first dimension (i.e., the node dimension) by one position to predict the partition indices of the next node, and we concatenate the known partitions of the current node to predict the next partition. Since the number of known partitions vary, so does the size of the input vectors. Therefore, we linearly project these vectors so that all the input vectors have the same dimension  $d_{model}$ . So, we have:

$$\mathbf{z}_{i,0}^0 = W_0^{in} [\mathbf{z}_{i-1,1}, \dots, \mathbf{z}_{i-1,C}], \quad (10)$$

and

$$\mathbf{z}_{i,c}^0 = W_c^{in} [\mathbf{z}_{i-1,1}, \dots, \mathbf{z}_{i-1,C}, \mathbf{z}_{i,1}, \dots, \mathbf{z}_{i,c}], \quad (11)$$

where the  $W_c^{in} \in \mathbb{R}^{d_{model} \times (d_{latent} + (c/C)d_{latent})}$  are matrices of parameters and  $[,]$  is the concatenation operator. To obtain the vector in the first position  $\mathbf{z}_{1,c}$ , we introduce a virtual node  $(\mathbf{z}_{0,1}, \dots, \mathbf{z}_{0,C})$  made of vectors of zeros.

After  $L$  layers, we project the output  $\mathbf{z}_{i,c}^L$  and apply softmax to model the index distribution of the next partition.

$$P_\theta(k_{i,c}) = \text{softmax}(f_{out}(\mathbf{z}_{i,c-1}^L)). \quad (12)$$

We pad the sequence with an end-of-sequence token so that the sequence can take various sizes. Since we sorted the indices in the training set, the indices lower than the last known index are out of the distribution, for instance  $p(k_{i,1} \geq k_{i-1,1}) = 0$ . Even though, the auto-regressive model should learn to generate the sequence following the order in the training set, we ease the task of our model by enforcing this constraint with masking.

### 4.2.3 Transformer

Transformer is based on attention. The attention function takes queries  $\mathbf{q}_i$ , keys  $\mathbf{k}_i$  and values  $\mathbf{v}_i$ , all are transformations from the corresponding representation  $\mathbf{z}_i$ . The attention output is a weighted sum of the values, where the weights correspond to a compatibility function, such as the scalar product, between queries and keys. The queries correspond to the aggregating position, while keys and values correspond to aggregated positions. The original attention from Vaswani et al. (2017) includes a scaling factor so that the attention output is computed as:

$$\mathbf{a}_i = \sum_{j \leq i} \text{softmax}\left(\frac{\mathbf{q}_i^T \mathbf{k}_j}{\sqrt{d_k}}\right) \mathbf{v}_j. \quad (13)$$

In practice, all attention functions are computed simultaneously using matrix multiplication. Masking  $M$  ensures that the weighted sum includes allowed positions only. We have:  $A = \text{softmax}\left(\frac{QK^T}{\sqrt{d_k}} \odot M\right)V$ . Following the original paper Vaswani et al. (2017), we use multi-head attention, residual connections, position-wise fully connected feed-forward networks, and positional encoding.

**2D Attention** The main idea behind 2D-Transformer lies in the computation of the attention function. Instead of computing the attention function for all the partitions, we compute it over the node embeddings as a whole. In addition to the benefits offered by transformers over other auto-regressive models, such as the computational complexity per layer, the parallelizable computation, and the short path lengths between long-range dependencies Vaswani et al. (2017), our 2D-Transformer implements parameter sharing for computational efficiency and better generalization. So, the keys and values are computed once for the whole node, so that we have:  $\mathbf{k}_i^l = f_k^l(\mathbf{z}_{i+1,0}^l)$ , and  $\mathbf{v}_i^l = f_v^l(\mathbf{z}_{i+1,0}^l)$ . One can interpret it as a form of parameter sharing since we use the same keys and values and, therefore, the same set of parameters for all the partitions. Nevertheless, the attention weights depend on the partition through the queries, which are different for each partition, as  $\mathbf{q}_{i,c}^l = f_{q,c}^l(\mathbf{z}_{i,c}^l)$ . In practice, the functions  $f_k$ ,  $f_v$ , and  $f_q$  are small neural networks.

Thanks to the queries, the attention score,  $\mathbf{q}_{i,c}^T \mathbf{k}_j$ , also depends on both dimensions. So, the main change of our model compared to the standard Transformer appears in the attention function, which we compute as:

$$\mathbf{a}_{i,c} = \sum_{j < i} \text{softmax}\left(\frac{\mathbf{q}_{i,c}^T \mathbf{k}_j}{\sqrt{d_k}}\right) \mathbf{v}_j. \quad (14)$$

Due to the unique key and value for the first dimension, we compute the summation along the second dimension only by including only the previous representations ( $j < i$ ). As the original Transformer, we scale the attention score by  $\sqrt{d_k}$ , where  $d_k$  is the dimensionality of the vector  $\mathbf{k}$ . The information about previous partitions in the current node passes through the residual connections as presented hereunder.

**Transformer blocks** Except for the attention function, our model follows the Transformer architecture. We compute attention in every head of every layer and use element-wise feed-forward neural network, layer normalization, as well as residual connections:

$$\mathbf{z}_{i,c}^{l+1} = \text{LayerNorm}(\tilde{\mathbf{a}}_{i,c}^l + f_z^l(\tilde{\mathbf{a}}_{i,c}^l)), \quad (15)$$

where

$$\tilde{\mathbf{a}}_{i,c}^l = \text{LayerNorm}(\mathbf{z}_{i,c}^l + [\mathbf{a}_{i,c}^l]_1^H) \quad (16)$$

, and where  $\square_1^H$  is the concatenation of the  $H$  heads. After  $L$  blocks, we take the outputs  $\mathbf{z}_{i,c}^{L+1}$  to model the probability distribution of the next index, as described in Equation 12.

### 4.3 Generation

For generation, we iteratively sample from  $p_\theta(k_{i,c})$ , and get the corresponding  $\mathbf{z}_{i,c}$ . Sequence generation stops upon sampling the end-of-sequence token or reaching the maximum number of node embeddings  $n_{max}$ . So, we can generate graphs of various sizes, and we need at most  $n_{max}C$  iterations to generate an instance.

Despite the auto-regressive method, generation with our model is significantly faster than other methods. There are three reasons for this. First, at each iteration, the computational complexity is bounded by the vector-matrix product  $q_{i,c}^T K^T$ , which is  $\mathcal{O}(d_{model}^2)$ , where most models require at least  $\mathcal{O}(n^w)$ , where  $w$  is the matrix multiplication exponent. Second, the length of the auto-regressive sequence for graphs usually depends on the number of (potential) edges and is proportional to  $n^2$ . Instead, our method is auto-regressive over a sequence depending linearly on  $n$ . For the current size of the generated graphs,  $nC$  is also smaller than the number of time steps in score-based models. We input the generated sets into the decoder and generate the resulting graphs simultaneously. Finally, the efficiency of our method allows us to keep the size of our model small. As presented in Appendix A.3, the largest hidden dimension of our experimental models never exceeds 256 hidden units, far from the dimension of current large models. In Section 5, we experimentally show that our method is comparatively fast at generation.

## 5 Evaluation

This Section presents the results of our experiments evaluating our model. We first compare the performance of our DGAE with baseline models, both on simple and annotated graphs. We then perform various ablation studies to evaluate and understand our model better.

### 5.1 Experimental setup

We evaluate our model on both synthetic datasets and molecular datasets. In the following, we present these datasets, the metrics used to assess the quality of generated samples, and the baseline models used for comparison. Appendix A.3 reports the details of the models, the hyperparameters choices and the resulting number of parameters used for the experiments. For a fair comparison, we adopt the experimental procedure followed in Jo et al. (2022) regarding metrics, split between training and test sets, number models and runs, and sample sizes described hereafter.

#### 5.1.1 Simple graphs

For simple graphs, we evaluated the performance of our model on two small datasets, namely Ego-Small and Community-Small, with 200 and 100 graphs, respectively. In particular, we split the datasets between training and test set with a ratio of 80%–20% as Jo et al. (2022) and use the exact same split when available.

The Ego-Small dataset is constructed by extracting ego-networks from the large citeseer network, a real-world social network. The dataset comprises 200 graphs having between 4 and 18 nodes.

---

The Community-Small dataset is purely synthetic. The number of nodes in each graph is uniformly sampled from the set  $\{12, 14, 16, 18, 20\}$ . Each graph is divided into two communities of equal size. The probability of edge intra-community is set to  $p_{intra} = 0.7$ , while the probability of edge between inter-communities is set to  $p_{inter} = 0.03$ , with the constraint of having at least one edge between communities. We use the version of the dataset proposed by Jo et al. (2022) containing 100 graphs.

Enzymes is a dataset containing 587 protein graphs that represent the protein tertiary structures of enzymes. It is extracted from the BRENDA database. The graphs in this dataset are larger than in Ego-small and Community-Small, with a node range between 10 and 125.

We employ the maximum mean discrepancy (MMD) to compare the distributions of graph statistics between generated and test graphs You et al. (2018). The MMDs are computed over the distributions of degrees (deg.), clustering coefficients (clust.), and the number of occurrences of orbits with up to four nodes (orbit)<sup>3</sup>. Similar to Jo et al. (2022), we utilize the Gaussian Earth Mover’s Distance (EMD) kernel to compute the MMDs.

The MMDs are computed by comparing the test set to generated samples of the same size as the test set. For Ego-Small and Community-Small, our reported results are the average of fifteen runs, i.e., fifteen generation batches with the test set size used for evaluation against the test set: three runs from five models trained independently. For the Enzymes dataset, which contains much larger graphs, we follow Jo et al. (2022) and average over three runs from a single model. Due to space limitation, we report the standard deviation in the appendix B.

### 5.1.2 Molecular datasets

We evaluated the performance of our model on two widely used datasets for molecule generation: Qm9 Ramakrishnan et al. (2014) and Zinc250k Irwin et al. (2012).

The Qm9 dataset Ramakrishnan et al. (2014) comprises 133,885 small organic molecules with up to nine heavy atoms, consisting of only four atom types, namely  $C, O, N, F$ . We followed the convention in previous works and employed the kekulized version of the dataset with three edge types (single, double, and triple).

The Zinc250k dataset is a subset of the Zinc database Irwin et al. (2012) that includes 250,000 molecules with up to 38 heavy atoms of nine types. We also used the kekulized representation of this dataset.

We used the test sets provided by Jo et al. (2022). The metrics are calculated over 10,000 samples from training and test sets when needed.

Traditionally, molecule generation was evaluated through three metrics: validity, uniqueness, and novelty. We argue that these metrics are unsuitable for evaluating the generative graph models.

Recent works mostly use valency corrections, bringing the validity rate to 100%. Consequently, this metric has become uninformative. Uniqueness and novelty primarily indicate potential mode collapse and overfitting, respectively. Since most models, including ours, achieve a high score, these metrics provide little information for evaluation. Therefore, we do not use these metrics for evaluation. Nonetheless, we report them in the Appendix B for completeness.

Instead, we use the Fréchet ChemNet Distance (FCD) Preuer et al. (2018) and the Neighborhood subgraph pairwise distance kernel (NSPDK) MMD Costa & Grave (2010) metrics. As highlighted in Jo et al. (2022) *‘FCD and NSPDK MMD are salient metrics that assess the ability to learn the distribution of the training molecules, measuring how close the generated molecules lie to the distribution’*. FCD assesses the generated molecules in chemical space, while NSPDK MMD evaluates the distribution of the graph structures.

In addition to FCD and NSPDK metrics, we also include the validity rate without correction as a supplementary evaluation metric. This metric calculates the fraction of valid molecules without any valency correction or edge resampling, and we employ the version that allows for formal charge as in Jo et al. (2022).

---

<sup>3</sup>We remind that an orbit is the equivalence class of nodes of a graph under the action of its automorphisms. Less formally, it is a set of nodes that are structurally similar. In Figure 13 of appendix D, the nodes with the same color belong to the same orbit

---

## 5.2 Baseline models

We present the results of six baseline models in our experiments for simple graphs, three sequential and three permutation-equivariant models. The first model, GraphRNN You et al. (2018), is an RNN-based auto-regressive model and is the paper that introduced the experiments and metrics we use. The second model, GraphDF Luo et al. (2021), is a discrete flow-based model and GraphARM Kong et al. (2023) is the recent diffusion-based sequential model. The third and fourth models are one-shot continuous diffusion models, namely EDP-GNN Yang et al. (2019) and GDSS Jo et al. (2022). EDP-GNN is initially designed for simple graphs, while GDSS can generate both simple and annotated graphs. Finally, Digress Vignac et al. (2023) is a discrete diffusion model.

In addition to these models, we randomly sample the same number of graphs from the training set as in the test set to use as a baseline. It gives us the distance between two random samples from the true distribution. Models under this baseline indicate that the generated sample overfits the test set. We report the average MMDs between the test set and 15 random samples drawn from the training set.

For molecular graphs, we also present the results of six baseline models. We utilize GraphAF, GraphDF Luo et al. (2021) and GraphARM. Additionally, we compare our model against MoFlow Zang & Wang (2020), a one-shot flow-based model, EDP-GNN Yang et al. (2019) a score-based model adapted by Jo et al. (2022) to handle annotated graphs, GDSS Jo et al. (2022), another score-based model and Digress Vignac et al. (2023), a discrete diffusion model. We take the results from Jo et al. (2022) for all baselines except GraphARM and Digress taken from Kong et al. (2023).

As discussed in Section 3, there are models specifically designed for graph generation using different types of representation. In particular, some recent models, such as E(3) Equivariant Diffusion Model (EDM) and Geometric Latent Diffusion Models (GEOLDM) leverage diffusion models representing molecules as 3D coordinates point clouds. These models predict the connections between atoms post hoc based on the distance between atoms. Compared to our experiments, these models use additional domain-knowledge information, particularly the atom positions. So, they must use datasets including this information, such as Qm9, but excluding Zinc250k. Moreover, they use specific metrics such as atom and molecule stability. Conversely, they do not report specific metrics for graphs such as NSPDK. Consequently, the only point of comparison is the validity rate on QM9. On this metric, EDM and GEOLDM obtain close and comparable results with the models used as baselines for our experiment with 91.9% and 93.8%, respectively.

## 5.3 Results

This Section reports quantitative evaluation of the experiments. We provide visualization of the generated graphs in Appendix C.

We give the evaluation results on Ego-Small and Community-Small datasets in Table 1. In the case of Ego-Small, which is a relatively small and straightforward dataset, we observe that our model matches the scores obtained with random samples from the training set. GDSS Jo et al. (2022) also reaches this level (or better!) on all metrics. Therefore, this dataset does not allow to discriminate between the best models.

On the Community-Small dataset, our model outperforms all baseline models in all evaluation metrics. We attribute this success to the effectiveness of our proposed DGAE model.

Table 2 presents the results on the Enzymes datasets. Again, our model outperforms all baseline models on average. Only GraphRNN does slightly better on the degree MMD.

### 5.3.1 Molecular graphs

As presented in Table 3, our DGAE model exhibits superior performance to all other models regarding FCD and NSPDK metrics, frequently surpassing them by a substantial margin. Moreover, it is competitive with the baselines regarding validity without correction. The results suggest that our model performs better at capturing global graph features, as reported by the FCD and the NSPDK metrics while remaining competitive at capturing the local node-edge interactions necessary to generate valid molecules.



Table 1: MMDs distances based on degrees (deg.), clustering coefficients (clust.), and the number of occurrences of orbits with four nodes (orbit) and their averages (avg.) on datasets of small simple graphs.

		Ego-Small				Community-Small			
<b>Model</b>		<b>Deg.↓</b>	<b>Clust.↓</b>	<b>Orbit↓</b>	<b>Avg↓</b>	<b>Deg.↓</b>	<b>Clust.↓</b>	<b>Orbit↓</b>	<b>Avg↓</b>
	Training set	0.022	0.043	0.0062	0.024	0.015	0.026	0.0032	0.015
Auto-reg.	GraphRNN	0.090	0.220	<b>0.003</b>	0.104	0.080	0.120	0.040	0.080
	GraphDF	0.04	0.13	0.01	0.060	0.06	0.12	0.03	0.070
	GraphARM	0.019	0.017	0.010	<b>0.015</b>	0.034	0.082	<b>0.004</b>	0.040
One-shot	EDP-GNN	0.052	0.093	0.007	0.051	0.053	0.144	0.026	0.074
	GDSS	0.021	<b>0.024</b>	0.007	0.017	0.045	0.086	0.007	0.046
	DiGress	<b>0.015</b>	0.029	0.005	0.016	0.047	<b>0.041</b>	0.026	0.038
Ours	DGAE	0.021	0.041	0.007	0.023	<b>0.032</b>	0.062	0.0046	<b>0.033</b>

Table 2: MMDs distances based on degrees (deg.), clustering coefficients (clust.), and the number of occurrences of orbits with up to four nodes (orbit) and their averages (avg.) on the Enzymes dataset.

		Enzymes			
<b>Model</b>		<b>Deg.↓</b>	<b>Clust.↓</b>	<b>Orbit↓</b>	<b>Avg↓</b>
	Training set	0.004	0.021	0.001	0.008
Auto-reg.	GraphRNN	0.017	0.062	0.046	0.042
	GraphDF	1.503	1.061	0.202	0.922
	GraphARM	0.029	0.054	0.015	0.033
One-shot	EDP-GNN	0.052	0.093	0.007	0.051
	GDSS	0.026	0.061	0.009	0.032
	DiGress	<b>0.004</b>	0.083	<b>0.002</b>	0.030
Ours	DGAE	0.020	<b>0.051</b>	0.003	<b>0.025</b>

Table 3: MMD distances based Neighborhood subgraph pairwise distance kernel (NSPDK) and Fréchet ChemNet Distance on the Qm9 and Zinc250k datasets.

		Qm9			Zinc		
<b>Model</b>		<b>NSPDK↓</b>	<b>FCD↓</b>	<b>Valid. %↑</b>	<b>NSPDK↓</b>	<b>FCD↓</b>	<b>Valid. %↑</b>
auto-reg.	GraphAF	0.021	5.53	74.4	0.044	16.0	68.5
	GraphDF	0.064	10.92	93.88	0.177	33.5	90.6
	MoFlow	0.017	4.47	91.4	0.046	20.9	63.1
One-shot	EDP-GNN	0.005	2.68	47.5	0.049	16.7	83.0
	GDSS	0.003	2.90	95.7	0.019	14.7	<b>97.0</b>
	DiGress	<b>0.0005</b>	<b>0.36</b>	<b>99.0</b>	0.082	23.1	91.0
Ours	DGAE	0.0015	0.86	92.0	<b>0.007</b>	<b>4.4</b>	77.9

---

### 5.3.2 Generation time

Finally, we use the Zinc dataset to assess the generation time of our model. We compare it against the best auto-regressive model Luo et al. (2021) and the best one-shot model Jo et al. (2022). We compute the clock time to generate 1000 graphs in the rdkit format on one GeForce RTX 3070 GPU and 12 CPU cores. We report the result in Table 4.

Our model is several orders of magnitude faster than the two baseline models. Our model not only presents very high performances at modeling graph distribution, but it is also much faster at generation.

Table 4: Generation time in seconds to generate 1000 graphs with models trained on molecular datasets .

Models	Time (s)	
	Qm9 ↓	Zinc ↓
GraphDF	3791.67	3859.23
GDSS	28.07	300.44
DiGress	54.01	799.43
DGAE (Ours)	<b>0.33</b>	<b>1.80</b>

### 5.4 Ablation study

We run two types of ablation studies. First, we empirically observe the effect of the various types of data augmentation. We then evaluate the effect of the codebooks and partition size. For all the ablation studies, we use the Zinc250k dataset, which is by far the largest dataset used for the experiments (regarding the number of graphs).

#### 5.4.1 Graph Features Augmentation

Numerous feature augmentation strategies for graphs have been proposed to overcome the inherent constraints of GNNs (see Section 4.1.2 and 2.4). Using such feature augmentations for graph generation has become a prevalent practice. However, we are not aware of any work evaluating these methods in generative modeling. The primary objective of these auxiliary features is to enhance the identification of graph features. A convenient way of evaluating a model’s capability of capturing graph features and substructures is by assessing its reconstruction accuracy. Thus, we evaluate the methods for synthetic graph feature methods based on their reconstruction performance.

Therefore, we have conducted a comparative analysis of several feature augmentation techniques, including spectral embedding, cycle counts, random features, and our  $p$ -paths method. The impact of each augmentation is evaluated independently against a scenario where no augmentation is applied. Further, we assess the impact of omitting one method compared to the combined use of all techniques. In figure 3, we report the reconstruction loss over 20 epochs.

When used alone, the reconstruction loss curves suggest that the spectral embedding and our  $p$ -paths method dramatically improve the reconstruction loss. Conversely, the cycle count and random feature techniques demonstrate negligible, if any, effects. Upon removal of a single method, the performance degradation is most noticeable in the absence of our  $p$ -path method. The effect is also evident for the random and spectral features. Conversely, the cycle count contributes marginally, if at all, to the overall effect. We conclude that our feature augmentation method is effective at enhancing MPNN as feature extractor on the node neighborhood, showing competitive performance against the computationally expensive method using spectral features.

In table 5, we present the impact of the feature augmentation on the pre-processing time and the training times. We measure the pre-processing time, i.e., the time to transform the dataset stored as a numpy object to a pytorch-geometric dataset, including the augmented features. We also compute the time for 1000 training iterations, i.e., 1000 parameter updates. For both, we compare our  $p$ -path method alone against

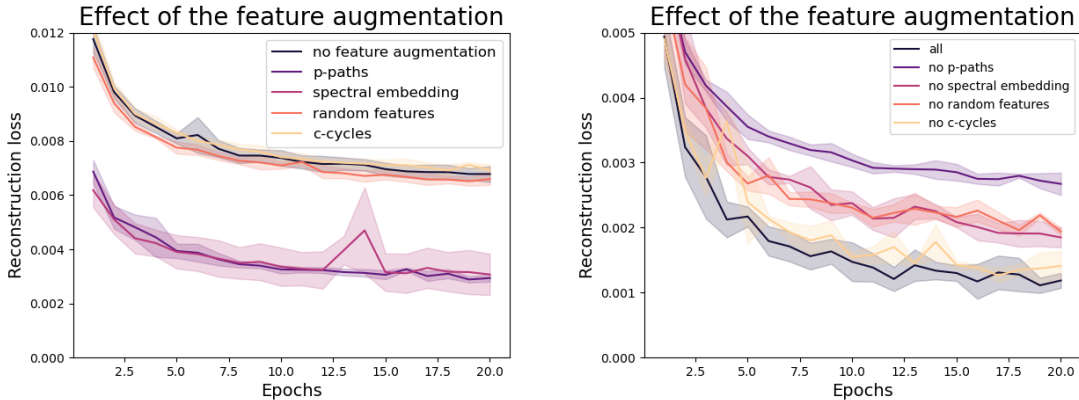


Figure 3: The lines represent the average over three runs and the shaded area the standard deviation.

the dataset without feature augmentation and with the spectral feature. We report the clock time measured on the Zinc250k dataset with one GeForce RTX 3070 GPU and 12 CPU cores.

Table 5: Pre-processing and training time for some feature augmentation methods in seconds. We compute the training time over 1000 training iterations.

Methods	Time (s)	
	Pre-processing ↓	Training ↓
No augmentation	74.81	38.19
Spectral feature	151.22	38.09
$P$ -path feature (ours)	231.18	38.71

We observe that the pre-processing time for our  $p$ -path scheme is significantly slower than the pre-processing without feature augmentation and the method based on spectral features. Nevertheless, the method remains short in comparison to the training time of graph generative models, which typically spans hours, if not days. Regarding the training, all methods are very close, our  $p$ -path being marginally slower.

#### 5.4.2 Influence of Codebook Sizes and Partitioning

This section evaluates the impact of varying the codebook and partitioning sizes. We first evaluate their effect on dictionary usage. We then study the effects on the autoencoder training *and* the prior training, given that the size of the codebook and the partitioning determine both the length of the auto-regressive sequence ( $nC$ ) and the dimensionality of the categorical distribution<sup>4</sup> ( $m+1$ ). For these experiments run on the Zinc250k dataset, we compare ten configurations for various codebook size  $m$  and number of partition  $C$ , representing three sizes of possible codeword sequences  $M$ :  $256^1 = 16^2 = 4^4$ ,  $1024^1 = 32^2 \approx 10^3$ , and  $4096^1 = 64^2 = 16^3 = 8^4$ .

We first analyze the dictionary usage, reporting the normalized perplexity. The perplexity is a measure of the dictionary usage computed as  $e^{H(P(z_i^q))}$ , where  $H(P(z_i^q))$  is the entropy over the dictionary likelihood. The closer the distribution is to the uniform distribution, the higher the perplexity. The maximum of perplexity corresponds to the dictionary size  $M$ . To compare various dictionary sizes, we use the normalized perplexity  $\frac{1}{M} e^{H(P(z_i^q))}$ . We present the result in Figure 4. We see that the normalized perplexity slightly decreases as the dictionary size increases. We also see that using a single large codebook, in this case, a single codebook of size 4096, leads to codebook collapse.

We then assess the impact of the codebook size  $m$ , the number of partitions  $C$ , and the dictionary size (i.e. the number of possible codeword sequences  $M = m^C$ ), on the reconstruction loss of the auto-encoder. We

<sup>4</sup>The '+1' refers to the end-of-sequence token

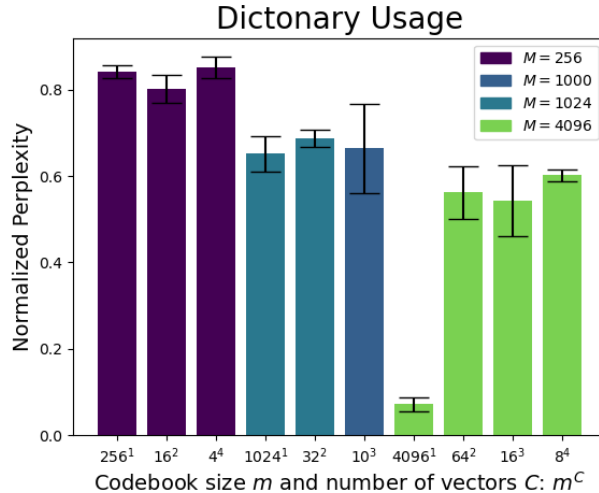


Figure 4: Effect of the codebook size and the partitioning on the dictionary usage. We report the normalized perplexity averaged over three runs. The black lines indicate the standard deviations.

analyze ten configurations for various codebook size  $m$  and number of partition  $C$ , representing three sizes of possible codeword sequences  $M$ :  $256^1 = 16^2 = 4^4$ ,  $1024^1 = 32^2 \approx 10^3$ , and  $4096^1 = 64^2 = 16^3 = 8^4$ . For comparison, we also include an experiment without quantization. We then selected the best reconstruction loss on the test set (calculated after each epoch) and reported the average across three runs. Figure 5 depicts the outcome. Our findings suggest that the number of possible sequences is critical, particularly when small (256 in our experiment). Conversely, the absence of quantization yield almost perfect reconstruction (so that its representation on Figure 5 is barely perceptible). However, the benefits of increasing the number of possible sequences become limited once its number surpasses a certain threshold. In this experiment, the advantage of increasing the number of possible sequences from 1024 to 4096 is unclear. Likewise, the partitioning effects become significant when the number of possible sequences is low, with smaller partitions proving more beneficial. However, the impact decreases with larger number of possible sequences. In our experiments, we do not see any effect when increasing the number of possible sequences to 4096. In Appendix C, we present similar figures reporting node and edge error rates. With dictionary size larger than 256, we reach close to perfect reconstruction, both error rates lying below 0.001 for almost all configurations.

We finally observe the effect on generation. We do not present the result without quantization because our 2D-Transformer require the sorted the quantized vectors for training. Therefore, our model is not able to perform generation without quantization. We report here the NSPDK metric, but the FCD, reported in Appendix C presents similar results. The benefits of large number of arrangements and small number of partitions vanish. The most significant observation is the poor result for  $m = 4096$  and  $C = 1$ . We assume that comes from codebook collapse observed in Figure 4, which results in a high probability of sampling indices out of the distribution. All the other settings result in comparable NSPDK values, which are lower than those of the baseline models. We also observe that the configuration with two partitions ( $C = 2$ ) and a codebook size of  $m = 32$  presents slightly better generation metrics than the other configurations.

## 6 Conclusion

Our work introduces DGAE, a powerful generative model for graph in two stages. In the first stage, we leverage an auto-encoder mapping graphs to sets and recovering graphs from sets. We use permutation-equivariant functions to prevent the difficulties caused by the multiple possible representations of graphs. In the second stage, we sort the sets into sequences, and learn them auto-regressively. In its present stage, we do not see any ethical concern with our model.

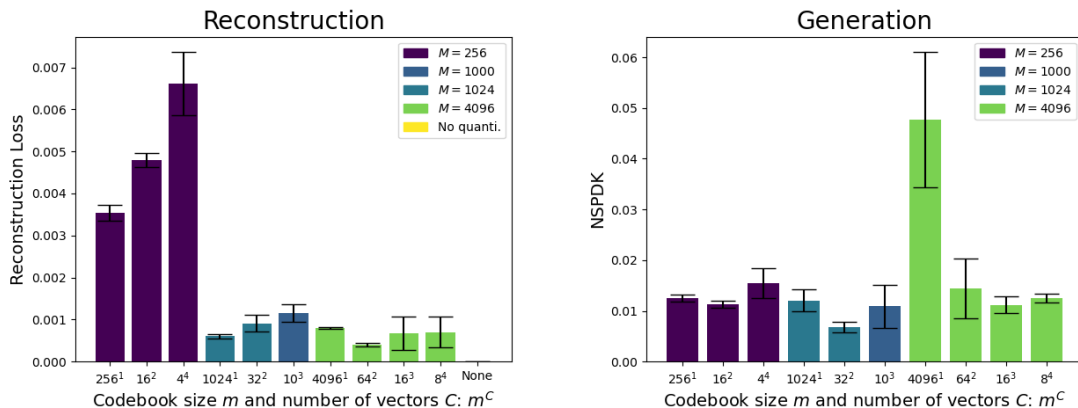


Figure 5: Effect of the codebook size and the partitioning on reconstruction (left) and generation (right). We report the best reconstruction loss and the best NSPDK averaged over 3 runs. The black lines indicate the standard deviations.

Our model achieve excellent performance at learning graph distributions. Our empirical evaluation shows that it outperforms baseline models, often by a large margin. Moreover, our model is order of magnitude faster at generation than competitive baseline models.

Implementing our model, we introduce two innovative techniques: a new feature augmentation method and a new Transformer architecture for sequential data over 2 dimensions.

However, our model presents also some limitations. First, our model requires two stages of training. This makes the hyperparameter tuning complicated, particularly for hyperparameters that influence both training stages, such as the number of partitions  $C$  or the codebook size  $m$  for instance. Second, our model cannot perform conditional generation yet. We hypothesize that conditioning the auto-regressive model might be sufficient. Nevertheless, the elaboration and validation of conditional generation remain topics for future investigation.

Lastly, addressing the challenge of scaling models to accommodate larger graphs is a prevalent concern in generative modeling, one that our model does not currently tackle. We have evaluated our model on graphs with up to 125 nodes. Adapting our model to handle larger graphs would raise challenges related to computation, memory, and overall model performance. This is another line of research open for further exploration.

Distinct from the two predominant approaches in current literature, i.e. the fully sequential and the fully permutation-equivariant methods, our generative model for graphs introduces an innovative and competitive framework. We view its present limitations as promising opportunities for future research.

## References

- V. Arvind, Frank Fuhlbrück, Johannes Köbler, and Oleg Verbitsky. On weisfeiler-leman invariance: Sub-graph counts and related graph properties. *Journal of Computer and System Sciences*, 113:42–59, 2020. ISSN 0022-0000. doi: <https://doi.org/10.1016/j.jcss.2020.04.003>. URL <https://www.sciencedirect.com/science/article/pii/S0022000020300386>.
- Yoann Boget, Magda Gregorova, and Alexandros Kalousis. Graph annotation generative adversarial networks. In Emtiyaz Khan and Mehmet Gonen (eds.), *Proceedings of The 14th Asian Conference on Machine Learning*, volume 189 of *Proceedings of Machine Learning Research*, pp. 16–16. PMLR, 12–14 Dec 2023. URL <https://proceedings.mlr.press/v189/boget23a.html>.
- Marc Brockschmidt, Miltiadis Allamanis, Alexander L. Gaunt, and Oleksandr Polozov. Generative code modeling with graphs. In *International Conference on Learning Representations*, 2019. URL <https://arxiv.org/abs/1907.00001>.

- 
- [//openreview.net/forum?id=Bke4KsA5FX](https://openreview.net/forum?id=Bke4KsA5FX).
- Bo Chen, Le Sun, and Xianpei Han. Sequence-to-Action: End-to-End Semantic Graph Generation for Semantic Parsing. *ACL 2018 - 56th Annual Meeting of the Association for Computational Linguistics, Proceedings of the Conference (Long Papers)*, 1:766–777, 2018. doi: 10.18653/V1/P18-1071. URL <https://aclanthology.org/P18-1071>.
- Zhengdao Chen, Lei Chen, Soledad Villar, and Joan Bruna. Can graph neural networks count substructures? In H. Larochelle, M. Ranzato, R. Hadsell, M.F. Balcan, and H. Lin (eds.), *Advances in Neural Information Processing Systems*, volume 33, pp. 10383–10395. Curran Associates, Inc., 2020. URL [https://proceedings.neurips.cc/paper\\_files/paper/2020/file/75877cb75154206c4e65e76b88a12712-Paper.pdf](https://proceedings.neurips.cc/paper_files/paper/2020/file/75877cb75154206c4e65e76b88a12712-Paper.pdf).
- Fabrizio Costa and Kurt De Grave. Fast neighborhood subgraph pairwise distance kernel. In Johannes Fürnkranz and Thorsten Joachims (eds.), *Proceedings of the 27th International Conference on Machine Learning (ICML-10), June 21-24, 2010, Haifa, Israel*, pp. 255–262. Omnipress, 2010. URL <https://icml.cc/Conferences/2010/papers/347.pdf>.
- Nicola De Cao and Thomas Kipf. MolGAN: An implicit generative model for small molecular graphs. *arXiv:1805.11973 [cs, stat]*, May 2018. URL <http://arxiv.org/abs/1805.11973>. arXiv: 1805.11973.
- Jiarui Feng, Yixin Chen, Fuhai Li, Anindya Sarkar, and Muhan Zhang. How powerful are k-hop message passing graph neural networks. In Alice H. Oh, Alekh Agarwal, Danielle Belgrave, and Kyunghyun Cho (eds.), *Advances in Neural Information Processing Systems*, 2022. URL <https://openreview.net/forum?id=nN3aVRQsxGd>.
- Nikhil Goyal, Harsh Vardhan Jain, and Sayan Ranu. Graphgen: A scalable approach to domain-agnostic labeled graph generation. In Yennun Huang, Irwin King, Tie-Yan Liu, and Maarten van Steen (eds.), *WWW '20: The Web Conference 2020, Taipei, Taiwan, April 20-24, 2020*, pp. 1253–1263. ACM / IW3C2, 2020. doi: 10.1145/3366423.3380201. URL <https://doi.org/10.1145/3366423.3380201>.
- Rafael Gómez-Bombarelli, Jennifer N. Wei, David Duvenaud, José Miguel Hernández-Lobato, Benjamín Sánchez-Lengeling, Dennis Sheberla, Jorge Aguilera-Iparraguirre, Timothy D. Hirzel, Ryan P. Adams, and Alán Aspuru-Guzik. Automatic Chemical Design Using a Data-Driven Continuous Representation of Molecules. *ACS Central Science*, 4(2):268–276, February 2018. ISSN 2374-7943. URL <https://doi.org/10.1021/acscentsci.7b00572>. Publisher: American Chemical Society.
- Harald Andrés Helfgott, Jitendra Bajpai, and Daniele Dona. Graph isomorphisms in quasi-polynomial time, 2017.
- Emiel Hoogeboom, Víctor Garcia Satorras, Clément Vignac, and Max Welling. Equivariant diffusion for molecule generation in 3D. In Kamalika Chaudhuri, Stefanie Jegelka, Le Song, Csaba Szepesvari, Gang Niu, and Sivan Sabato (eds.), *Proceedings of the 39th International Conference on Machine Learning*, volume 162 of *Proceedings of Machine Learning Research*, pp. 8867–8887. PMLR, 17–23 Jul 2022. URL <https://proceedings.mlr.press/v162/hoogeboom22a.html>.
- John Ingraham, Vikas Garg, Regina Barzilay, and Tommi Jaakkola. Generative models for graph-based protein design. In H. Wallach, H. Larochelle, A. Beygelzimer, F. d'Alché-Buc, E. Fox, and R. Garnett (eds.), *Advances in Neural Information Processing Systems*, volume 32. Curran Associates, Inc., 2019.
- Sergey Ioffe and Christian Szegedy. Batch normalization: Accelerating deep network training by reducing internal covariate shift. In Francis Bach and David Blei (eds.), *Proceedings of the 32nd International Conference on Machine Learning*, volume 37 of *Proceedings of Machine Learning Research*, pp. 448–456, Lille, France, 07–09 Jul 2015. PMLR. URL <https://proceedings.mlr.press/v37/ioffe15.html>.
- John J. Irwin, Teague Sterling, Michael M. Mysinger, Erin S. Bolstad, and Ryan G. Coleman. Zinc: A free tool to discover chemistry for biology. *Journal of Chemical Information and Modeling*, 52(7):1757–1768, 2012. doi: 10.1021/ci3001277. URL <https://doi.org/10.1021/ci3001277>. PMID: 22587354.

- 
- Wengong Jin, Regina Barzilay, and Tommi Jaakkola. Junction tree variational autoencoder for molecular graph generation. In Jennifer Dy and Andreas Krause (eds.), *Proceedings of the 35th International Conference on Machine Learning*, volume 80 of *Proceedings of Machine Learning Research*, pp. 2323–2332. PMLR, 10–15 Jul 2018. URL <https://proceedings.mlr.press/v80/jin18a.html>.
- Wengong Jin, Regina Barzilay, and Tommi Jaakkola. Hierarchical Generation of Molecular Graphs using Structural Motifs. In *37th International Conference on Machine Learning, ICML 2020*, volume PartF16814, pp. 4789–4798, 2020. ISBN 9781713821120. URL <https://github.com/wengong-jin/hgraph2graph>.
- Jaehyeong Jo, Seul Lee, and Sung Ju Hwang. Score-based Generative Modeling of Graphs via the System of Stochastic Differential Equations. *Proceedings of the 39th International Conference on Machine Learning*, 162:10362–10383, 2022. URL <https://github.com/harryjo97/GDSS>. <http://arxiv.org/abs/2202.02514>.
- Lukasz Kaiser, Samy Bengio, Aurko Roy, Ashish Vaswani, Niki Parmar, Jakob Uszkoreit, and Noam Shazeer. Fast decoding in sequence models using discrete latent variables. In Jennifer Dy and Andreas Krause (eds.), *Proceedings of the 35th International Conference on Machine Learning*, volume 80 of *Proceedings of Machine Learning Research*, pp. 2390–2399. PMLR, 10–15 Jul 2018. URL <https://proceedings.mlr.press/v80/kaiser18a.html>.
- Thomas N. Kipf and Max Welling. Variational graph auto-encoders. In *NeurIPS Workshop on Bayesian Deep Learning*, 2016. URL [http://bayesiandeeplearning.org/2016/papers/BDL\\_16.pdf](http://bayesiandeeplearning.org/2016/papers/BDL_16.pdf).
- Matthew Klawonn and Eric Heim. Generating Triples With Adversarial Networks for Scene Graph Construction. *Proceedings of the AAAI Conference on Artificial Intelligence*, 32(1):6992–6999, apr 2018. ISSN 2374-3468. doi: 10.1609/AAAI.V32I1.12321. URL <https://ojs.aaai.org/index.php/AAAI/article/view/12321>.
- Johannes Köbler, Uwe Schöning, and Jacobo Torán. *Introduction*, pp. 1–4. Birkhäuser Boston, Boston, MA, 1993.
- Lingkai Kong, Jiaming Cui, Haotian Sun, Yuchen Zhuang, B. Aditya Prakash, and Chao Zhang. Autoregressive diffusion model for graph generation. In Andreas Krause, Emma Brunskill, Kyunghyun Cho, Barbara Engelhardt, Sivan Sabato, and Jonathan Scarlett (eds.), *Proceedings of the 40th International Conference on Machine Learning*, volume 202 of *Proceedings of Machine Learning Research*, pp. 17391–17408. PMLR, 23–29 Jul 2023. URL <https://proceedings.mlr.press/v202/kong23b.html>.
- Igor Krawczuk, Pedro Abranches, Andreas Loukas, and Volkan Cevher. {GG}-{gan}: A geometric graph generative adversarial network, 2021. URL <https://openreview.net/forum?id=qiAxL3Xqx1o>.
- Matt J. Kusner, Brooks Paige, and José Miguel Hernández-Lobato. Grammar Variational Autoencoder. In *Proceedings of the 34th International Conference on Machine Learning*, pp. 1945–1954. PMLR, July 2017. URL <https://proceedings.mlr.press/v70/kusner17a.html>. ISSN: 2640-3498.
- Maksim Kuznetsov and Daniil Polykovskiy. MolGrow: A Graph Normalizing Flow for Hierarchical Molecular Generation. *Proceedings of the AAAI Conference on Artificial Intelligence*, 35(9):8226–8234, feb 2021. ISSN 2159-5399. doi: 10.48550/arxiv.2106.05856. URL <https://arxiv.org/abs/2106.05856v1>.
- Qimai Li, Zhichao Han, and Xiao-Ming Wu. Deeper insights into graph convolutional networks for semi-supervised learning. In *Proceedings of the Thirty-Second AAAI Conference on Artificial Intelligence (AAAI-18)*, pp. 3538 – 3545, Palo Alto, CA, 2018-02. Association for the Advancement of Artificial Intelligence. ISBN 978-1-57735-800-8. 32nd AAAI Conference on Artificial Intelligence / 30th Innovative Applications of Artificial Intelligence Conference / 8th AAAI Symposium on Educational Advances in Artificial Intelligence; Conference Location: New Orleans, LA; Conference Date: February 2-7, 2018.
- Y. Li, W. Ouyang, B. Zhou, K. Wang, and X. Wang. Scene graph generation from objects, phrases and region captions. In *2017 IEEE International Conference on Computer Vision (ICCV)*, pp. 1270–1279,

- 
- Los Alamitos, CA, USA, oct 2017. IEEE Computer Society. doi: 10.1109/ICCV.2017.142. URL <https://doi.ieeecomputersociety.org/10.1109/ICCV.2017.142>.
- Yujia Li, Oriol Vinyals, Chris Dyer, Razvan Pascanu, and Peter Battaglia. Learning deep generative models of graphs. In *ICLR 2018, 6th International Conference on Learning Representations*, feb 2018. URL <https://openreview.net/forum?id=Hy1d-ebAb>.
- Renjie Liao, Yujia Li, Yang Song, Shenlong Wang, Will Hamilton, David K Duvenaud, Raquel Urtasun, and Richard Zemel. Efficient Graph Generation with Graph Recurrent Attention Networks. In *Advances in Neural Information Processing Systems*, volume 32. Curran Associates, Inc., 2019. URL <https://proceedings.neurips.cc/paper/2019/hash/d0921d442ee91b896ad95059d13df618-Abstract.html>.
- Jenny Liu, Aviral Kumar, Jimmy Ba, Jamie Kiros, and Kevin Swersky. Graph normalizing flows. In *Advances in Neural Information Processing Systems*, volume 32, 2019.
- Qi Liu, Miltiadis Allamanis, Marc Brockschmidt, and Alexander L Gaunt. Constrained Graph Variational Autoencoders for Molecule Design. *The Thirty-second Conference on Neural Information Processing Systems*, 2018.
- Andreas Loukas. What graph neural networks cannot learn: depth vs width. In *International Conference on Learning Representations*, September 2019. URL <https://openreview.net/forum?id=B112bp4YwS>.
- Chengqiang Lu, Qi Liu, Qiming Sun, Chang Yu Hsieh, Shengyu Zhang, Liang Shi, and Chee Kong Lee. Deep Learning for Optoelectronic Properties of Organic Semiconductors. *Journal of Physical Chemistry C*, 124(13):7048–7060, apr 2020. ISSN 19327455. URL <https://pubs.acs.org/doi/abs/10.1021/acs.jpcc.0c00329>.
- Youzhi Luo, Keqiang Yan, and Shuiwang Ji. GraphDF: A Discrete Flow Model for Molecular Graph Generation. *Proceedings of the 38th International Conference on Machine Learning*, 139:7192–7203, 2021. URL <http://arxiv.org/abs/2102.01189>.
- Kaushalya Madhawa, Katushiko Ishiguro, Kosuke Nakago, and Motoki Abe. Graphnvp: An invertible flow model for generating molecular graphs, 2019.
- Haggai Maron, Heli Ben-Hamu, Hadar Serviansky, and Yaron Lipman. Provably powerful graph networks. In H. Wallach, H. Larochelle, A. Beygelzimer, F. d'Alché-Buc, E. Fox, and R. Garnett (eds.), *Advances in Neural Information Processing Systems*, volume 32. Curran Associates, Inc., 2019. URL [https://proceedings.neurips.cc/paper\\_files/paper/2019/file/bb04af0f7ecaee4aae62035497da1387-Paper.pdf](https://proceedings.neurips.cc/paper_files/paper/2019/file/bb04af0f7ecaee4aae62035497da1387-Paper.pdf).
- Christopher Morris, Martin Ritzert, Matthias Fey, William L. Hamilton, Jan Eric Lenssen, Gaurav Rattan, and Martin Grohe. Weisfeiler and leman go neural: Higher-order graph neural networks. In *33rd AAAI Conference on Artificial Intelligence, AAAI 2019, 31st Innovative Applications of Artificial Intelligence Conference, IAAI 2019 and the 9th AAAI Symposium on Educational Advances in Artificial Intelligence, EAAI 2019*, volume 33, pp. 4602–4609. AAAI Press, jul 2019. ISBN 9781577358091. doi: 10.1609/aaai.v33i01.33014602. URL [www.aaai.org](http://www.aaai.org).
- Kenta Oono and Taiji Suzuki. Graph neural networks exponentially lose expressive power for node classification. In *International Conference on Learning Representations*, 2020. URL <https://openreview.net/forum?id=S1ld02EFPr>.
- Kristina Preuer, Philipp Renz, Thomas Unterthiner, Sepp Hochreiter, and Günter Klambauer. Fréchet chemnet distance: A metric for generative models for molecules in drug discovery. *Journal of Chemical Information and Modeling*, 58(9):1736–1741, 2018. doi: 10.1021/acs.jcim.8b00234. PMID: 30118593.
- Raghunathan Ramakrishnan, Pavlo O. Dral, Matthias Rupp, and O. Anatole von Lilienfeld. Quantum chemistry structures and properties of 134 kilo molecules. *Scientific Data*, 1(1):140022, August 2014. ISSN 2052-4463. URL <https://www.nature.com/articles/sdata201422>. Number: 1 Publisher: Nature Publishing Group.



- 
- Ali Razavi, Aaron van den Oord, and Oriol Vinyals. Generating diverse high-fidelity images with vq-vae-2. In H. Wallach, H. Larochelle, A. Beygelzimer, F. d'Alché-Buc, E. Fox, and R. Garnett (eds.), *Advances in Neural Information Processing Systems*, volume 32. Curran Associates, Inc., 2019. URL [https://proceedings.neurips.cc/paper\\_files/paper/2019/file/5f8e2fa1718d1bbcadf1cd9c7a54fb8c-Paper.pdf](https://proceedings.neurips.cc/paper_files/paper/2019/file/5f8e2fa1718d1bbcadf1cd9c7a54fb8c-Paper.pdf).
- Bidisha Samanta, Bidisha@iitkgp Ac In, Abir De, Vicenç Gomez, Pratim Kumar Chattaraj, Niloy Ganguly, Manuel Gomez-Rodriguez, Jana Gourhari, and Kumar Chattaraj. NEVAE: A Deep Generative Model for Molecular Graphs \*. *Journal of Machine Learning Research*, 21:1–33, 2020.
- Franco Scarselli, Gori Marco, Tsoi Ah Chung, Hagenbuchner Markus, and Monfardini Gabriele. The Graph Neural Network Model. *IEEE Transactions on Neural Networks*, 20, jan 2009. URL <https://ieeexplore.ieee.org/document/4700287>.
- Chence Shi, Minkai Xu, Zhaocheng Zhu, Weinan Zhang, Ming Zhang, and Jian Tang. Graphaf: a flow-based autoregressive model for molecular graph generation. In *International Conference on Learning Representations*, 2020. URL <https://openreview.net/forum?id=S1esMkHYPr>.
- Martin Simonovsky and Nikos Komodakis. GraphVAE: Towards Generation of Small Graphs Using Variational Autoencoders. *arXiv:1802.03480 [cs]*, February 2018. URL <http://arxiv.org/abs/1802.03480>. arXiv: 1802.03480.
- Aaron van den Oord, Oriol Vinyals, and koray kavukcuoglu. Neural discrete representation learning. In I. Guyon, U. Von Luxburg, S. Bengio, H. Wallach, R. Fergus, S. Vishwanathan, and R. Garnett (eds.), *Advances in Neural Information Processing Systems*, volume 30. Curran Associates, Inc., 2017.
- Ashish Vaswani, Noam Shazeer, Niki Parmar, Jakob Uszkoreit, Llion Jones, Aidan N Gomez, Łukasz Kaiser, and Illia Polosukhin. Transformer: Attention is all you need. *Advances in Neural Information Processing Systems 30*, pp. 5998–6008, 2017. ISSN 10495258.
- Clément Vignac, Andreas Loukas, and Pascal Frossard. Building powerful and equivariant graph neural networks with structural message-passing. In H. Larochelle, M. Ranzato, R. Hadsell, M.F. Balcan, and H. Lin (eds.), *Advances in Neural Information Processing Systems*, volume 33, pp. 14143–14155. Curran Associates, Inc., 2020. URL [https://proceedings.neurips.cc/paper\\_files/paper/2020/file/a32d7eeaae19821fd9ce317f3ce952a7-Paper.pdf](https://proceedings.neurips.cc/paper_files/paper/2020/file/a32d7eeaae19821fd9ce317f3ce952a7-Paper.pdf).
- Clement Vignac, Igor Krawczuk, Antoine Siraudin, Bohan Wang, Volkan Cevher, and Pascal Frossard. Digress: Discrete denoising diffusion for graph generation. In *The Eleventh International Conference on Learning Representations*, 2023. URL <https://openreview.net/forum?id=UaAD-Nu86WX>.
- Keyulu Xu, Weihua Hu, Jure Leskovec, and Stefanie Jegelka. How powerful are graph neural networks? In *International Conference on Learning Representations*, 2019. URL <https://openreview.net/forum?id=ryGs6iA5Km>.
- Minkai Xu, Alexander S Powers, Ron O. Dror, Stefano Ermon, and Jure Leskovec. Geometric latent diffusion models for 3D molecule generation. In Andreas Krause, Emma Brunskill, Kyunghyun Cho, Barbara Engelhardt, Sivan Sabato, and Jonathan Scarlett (eds.), *Proceedings of the 40th International Conference on Machine Learning*, volume 202 of *Proceedings of Machine Learning Research*, pp. 38592–38610. PMLR, 23–29 Jul 2023. URL <https://proceedings.mlr.press/v202/xu23n.html>.
- Carl Yang, Peiye Zhuang, Wenhan Shi, Alan Luu, and Pan Li. Conditional Structure Generation through Graph Variational Generative Adversarial Nets. In *Advances in Neural Information Processing Systems*, volume 32, 2019.
- Jiaxuan You, Rex Ying, Xiang Ren, William Hamilton, and Jure Leskovec. GraphRNN: Generating Realistic Graphs with Deep Auto-regressive Models. In *Proceedings of the 35th International Conference on Machine Learning*, pp. 5708–5717. PMLR, July 2018. URL <https://proceedings.mlr.press/v80/you18a.html>. ISSN: 2640-3498.

---

Seongjun Yun, Minbyul Jeong, Raehyun Kim, Jaewoo Kang, and Hyunwoo J Kim. Graph transformer networks. In H. Wallach, H. Larochelle, A. Beygelzimer, F. d'Alché-Buc, E. Fox, and R. Garnett (eds.), *Advances in Neural Information Processing Systems*, volume 32. Curran Associates, Inc., 2019. URL [https://proceedings.neurips.cc/paper\\_files/paper/2019/file/9d63484abb477c97640154d40595a3bb-Paper.pdf](https://proceedings.neurips.cc/paper_files/paper/2019/file/9d63484abb477c97640154d40595a3bb-Paper.pdf).

Chengxi Zang and Fei Wang. MoFlow: An Invertible Flow Model for Generating Molecular Graphs. *Proceedings of the ACM SIGKDD International Conference on Knowledge Discovery and Data Mining*, 10: 617–626, aug 2020. doi: 10.1145/3394486.3403104. URL <https://dl.acm.org/doi/10.1145/3394486.3403104>.

Adrian Łańcucki, Jan Chorowski, Guillaume Sanchez, Nanxin Marxer, Ricard and Chen, Doling Hans J.G.A., Sameer Khurana, Tanel Alumäe, and Antoine Laurent. Robust training of vector quantized bottleneck models. *arXiv:2005.08520 [cs, stat]*, May 2020. URL <https://arxiv.org/abs/2005.08520>.

---

## A Model Implementation Details

In this section, we provide more details on the implementation of our model used for the experiments.

### A.1 Decoder Output

For simple graphs, the edge representation  $e_{i,j}^L$  after the last layer  $L$  is a scalar, which we pass through a sigmoid function  $\sigma$ . The result is interpreted as the probability of the presence of an edge  $\sigma(e_{i,j}^L) = p_\theta(\epsilon_{i,j} = 1 | \mathcal{Z}^q)$ . In the case of annotated graphs with discrete attributes, the outputs corresponding to each node  $\mathbf{x}_i^L \in \mathbb{R}$  and each edge  $e_{i,j}^L \in \mathbb{S}$  are passed through a softmax function  $\sigma$ , yielding the probability distribution over their attributes, i.e.,  $\text{softmax}(\mathbf{e}_{i,j}^L) = p_\theta(\mathbf{e}_{i,j} | \mathcal{Z}^q)$  and  $\text{softmax}(\mathbf{x}_i^L) = p_\theta(\mathbf{x}_i | \mathcal{Z}^q)$ . Note that for edges, the absence of an edge has to be encoded as one of the output category.

Our model output different value for  $e_{i,j}$  and  $e_{j,i}$ . So, we can model directed graph. For undirected graphs, we enforce the symmetry of the adjacency by averaging the output matrix by its transpose.

For sampling, we always chose the mode of the discrete distribution  $\hat{x}_i = \text{argmax}_{\{r \in \mathbb{N}: r \leq R\}} (p_\theta(x_{i,r} | \mathcal{Z}^q))$  and  $\hat{e}_{i,j} = \text{argmax}_{\{s \in \mathbb{N}: s \leq S\}} (p_\theta(e_{i,j,s} | \mathcal{Z}^q))$ .

### A.2 Auto-encoder Training

**Codebooks initialization** The codebook initialization is important for the training quality of the auto-encoder. As proposed by Łańcucki et al. (2020), we initiate the auto-encoder training for  $T_{init}$  steps without quantization. Next, we collect  $S$  node embeddings,  $S$  being an hyperparameter, and perform  $k$ -means++ clustering. We use the resulting vectors as initial codebook vectors. We use  $S = 100K$  samples. Unlike Łańcucki et al. (2020), we do not re-estimate the codebook vector periodically. After initialization, we continue to update the codebooks thanks to a dedicated loss function details in Section 4.1.5.

**Reconstruction loss** We define the reconstruction loss as the negative log-likelihood. In practice, we use the binary cross-entropy loss for simple graphs and the cross-entropy loss for annotated graphs.

Also, for annotated graphs, the respective weight of the nodes and the edges in the loss function is an hyperparameter choice. In practice, for all our experiments, we use a constant weight for the edges and the nodes. For instance, for a graph with categorical distributions over nodes and edges, we used:

$$\mathcal{L}_{\text{recon.}} = \frac{1}{n + n^2} \left( \sum_{i=1}^n \sum_{r=1}^R x_{i,r} \ln(\tilde{x}_{i,r}) + \sum_{i=1}^n \sum_{\substack{j=1 \\ j \neq i}}^n \sum_{s=1}^S e_{i,j,s} \ln(\tilde{e}_{i,j,s}) \right), \quad (17)$$

where  $R$  and  $S$  are distribution supports of the node and the edge, respectively. The reconstruction loss can be easily modify to fit multiple variables per node and edge.

**Commitment loss** To prevent the expansion of the encoder outputs, we incorporate a regularization, similar to van den Oord et al. (2017), which keeps the learnt representations close to the cluster centers. We define it as the mean square distance between the partition vector and its corresponding codeword:

$$\mathcal{L}_{\text{commit.}} = \frac{1}{nC} \sum_{i=1}^n \sum_{c=1}^C \|\mathbf{z}_{i,c}^h - \text{sg}[\mathbf{z}_{i,c}^q]\|_2^2. \quad (18)$$

### A.3 Hyperparameters

Table 6: Parameters shared across experiments.

Data	Features augmentation	all
GNNs	layers in the neural networks	3
	activation function	ReLu
	Size of the hidden representations $e_{i,j}^l$ and $x_i^l$	32
Quantizer	partitions $C$	2
	latent vector size	8
	$\beta$ (loss commitment cost)	0.25
	$\gamma$ (loss weight)	0.1
Training	betas (adam optimizer)	0.9, 0.99
	learning rate decay	0.5
2d-transformer	heads in multihead att.	16
	layers in the neural networks	4
	units in the hidden layers of the mlp’s	$2 \times d_{models}$
	activation function	ReLu

Table 7: Parameters for the various experiments.

	dataset	Zinc	Qm9	Ego	Com-ity	Enzymes
GNNs	number of GNN layers	4	4	2	2	6
	units in mlp’s hidden layers	128	128	64	64	128
Quantizer	codebook size $K$	32	16	8	16	32
	initialization steps	1000	1000	0	0	100
Training	batch size	32	32	32	32	16
	param. updates between decay	25k	25k	10k	10k	10k
2d-transformer	blocks	6	6	3	3	6
	$d_{model}$	256	128	64	64	128

Table 8: Number of parameters in our experimental models

Datasets	Zinc	Qm9	Ego	Community	Enzymes
Auto-encoder	749K	746K	107k	107	1.14M
2D-Transformer	75.4M	18.9M	2.47M	2.47M	18.9M
Total	76.2M	19.7M	2.58M	2.58M	20.1M

## B Detailed results

All results in this section, except DGAE, are taken from Jo et al. (2022). Unfortunately, the results for GraphARM and DiGress are taken from Kong et al. (2023), which do not produce the standard deviation. So, we do not have more information than the ones produced in the core of the text.

### B.1 Qm9

Results are the means and the standard deviations of 3 runs.

Table 9: Generation results on the **Qm9** dataset.

Model	NSPDK↓	FCD↓	Val. wo. corr. %↑
GraphAF	0.021 ± 0.003	5.53 ± 0.40	74.4 ± 2.6
GraphDF	0.064 ± 0.000	10.92 ± 0.0	93.8 ± 4.8
MoFlow	0.017 ± 0.003	4.47 ± 0.60	91.4 ± 1.2
EDP-GNN	0.005 ± 0.001	2.68 ± 0.22	47.5 ± 3.6
GDSS	0.003 ± 0.000	2.90 ± 0.28	95.7 ± 0.8
DGAE	0.0015 ± 0.0000	0.86 ± 0.02	92.0 ± 0.25

Table 10: Generation results on the **Qm9** dataset.

Model	Uniqueness↓	Novelty↓	Validity %↑
GraphAF	88.64 ± 2.37	86.59 ± 1.95	100.00 ± 0.00
GraphDF	98.58 ± 0.25	98.54 ± 0.48	100.00 ± 0.00
MoFlow	98.65 ± 0.25	94.72 ± 0.77	100.00 ± 0.00
EDP-GNN	99.25 ± 0.05	86.58 ± 1.85	100.00 ± 0.00
GDSS	98.46 ± 0.61	86.27 ± 2.29	100.00 ± 0.00
DGAE	97.61 ± 0.17	79.09 ± 0.42	100.00 ± 0.00

## B.2 Zinc

Results are the means and the standard deviations of 3 runs.

Table 11: Generation results on the **Zinc** dataset.

Model	NSPDK↓	FCD↓	Val. wo. corr. %↑
GraphAF	0.044 ± 0.005	16.0 ± 0.5	68.5 ± 1.0
GraphDF	0.177 ± 0.001	33.5 ± 0.2	90.6 ± 4.3
MoFlow	0.046 ± 0.002	20.9 ± 0.2	63.1 ± 5.2
EDP-GNN	0.049 ± 0.006	16.7 ± 1.3	83.0 ± 2.7
GDSS	0.019 ± 0.001	14.7 ± 0.7	97.0 ± 0.8
DGAE	0.007 ± 0.000	4.4 ± 0.0	77.9 ± 0.5

Table 12: Generation results on the **Zinc** dataset.

Model	Uniqueness↓	Novelty↓	Validity %↑
GraphAF	98.64 ± 0.69	99.99 ± 0.01	100.00 ± 0.00
GraphDF	99.63 ± 0.01	100.00 ± 0.00	100.00 ± 0.00
MoFlow	99.99 ± 0.01	100.00 ± 0.00	100.00 ± 0.00
EDP-GNN	99.79 ± 0.08	100.00 ± 0.00	100.00 ± 0.00
GDSS	99.64 ± 0.13	100.00 ± 0.00	100.00 ± 0.00
DGAE	99.94 ± 0.03	99.97 ± 0.01	±100.00 ± 0.00

## B.3 Ego-small

For Ego-small, we only have the standard deviation for GDSS and our own model. Results are the means and the standard deviations of 15 runs, 3 different runs for 5 independently trained models.

Table 13: Generation results on the **Ego-Small** datasets.

Model	Degrees↓	Cluster.↓	Orbits↓
GDSS	0.021 ± 0.008	0.024 ± 0.007	0.007 ± 0.005
DGAE (Ours)	0.021 ± 0.010	0.041 ± 0.026	0.007 ± 0.005

#### B.4 Community-small

For Ego-small, we only have the standard deviation for GDSS and our own model. Results are the means and the standard deviations of 15 runs, 3 different runs for 5 independently trained models.

Model	Degrees↓	Cluster.↓	Orbits↓
GDSS	0.045 ± 0.028	0.086 ± 0.022	0.007 ± 0.004
DGAE (Ours)	0.032 ± 0.019	0.062 ± 0.032	0.0046 ± 0.004

Table 14: Generation results on the **Community-Small** dataset.

#### B.5 Enzymes

Results are the means and the standard deviations of 3 runs.

Table 15: Generation results on **Enzymes** datasets.

Model	Deg.↓	Clust.↓	Orbit↓
GraphRNN	<b>0.017</b> ± 0.007	0.062 ± 0.020	0.046 ± 0.031
GraphDF	1.503 ± 0.011	1.061 ± 0.011	0.202 ± 0.002
EDP-GNN	0.023 ± 0.012	0.268 ± 0.164	0.082 ± 0.078
GDSS	0.026 ± 0.008	0.061 ± 0.010	0.009 ± 0.005
DGAE (Ours)	0.020 ± 0.004	<b>0.051</b> ± 0.017	<b>0.003</b> ± 0.001

#### B.6 Generation time

Results are the means and the standard deviations of 3 runs.

Table 16: Generation time on molecular datasets in seconds.

Model	Time (s)	
	Qm9 ↓	Zinc ↓
GraphDF	3791.67 ± 16.21	3859.23 ± 8.34
GDSS	28.07 ± 0.15	300.44 ± 1.94
DiGress	54.01 ± 1.02	799.43 ± 38.22
DGAE (Ours)	<b>0.33 ± 0.01</b>	<b>1.80 ± 0.01</b>

---

## C Visualization

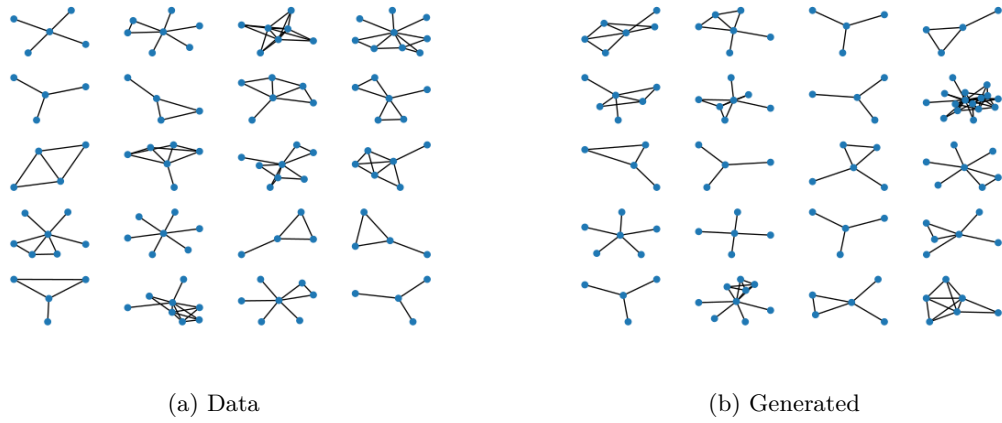


Figure 6: Example of graphs from the Ego-Small dataset and from generated samples.

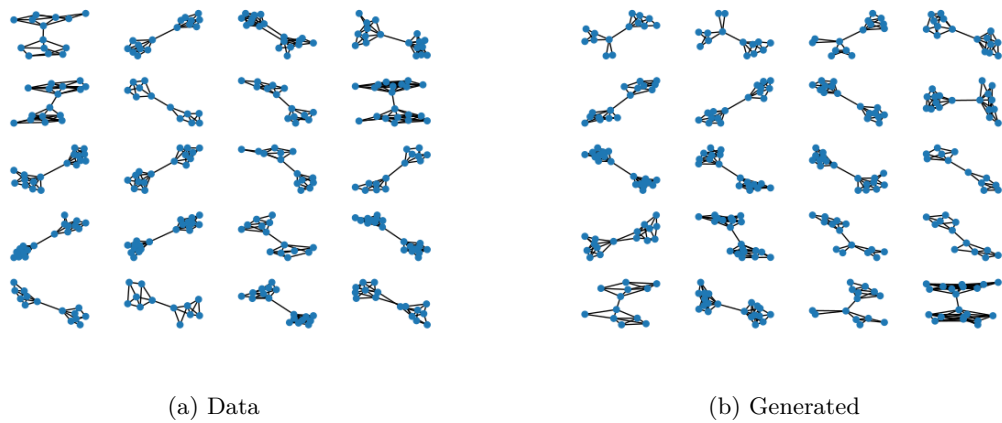


Figure 7: Example of graphs from the Community-Small dataset and from generated samples.

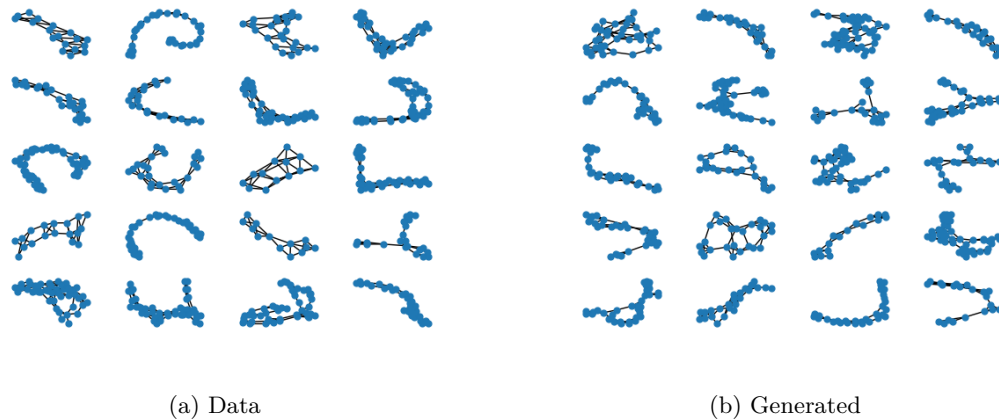


Figure 8: Example of graphs from the Community-Small dataset and from generated samples.

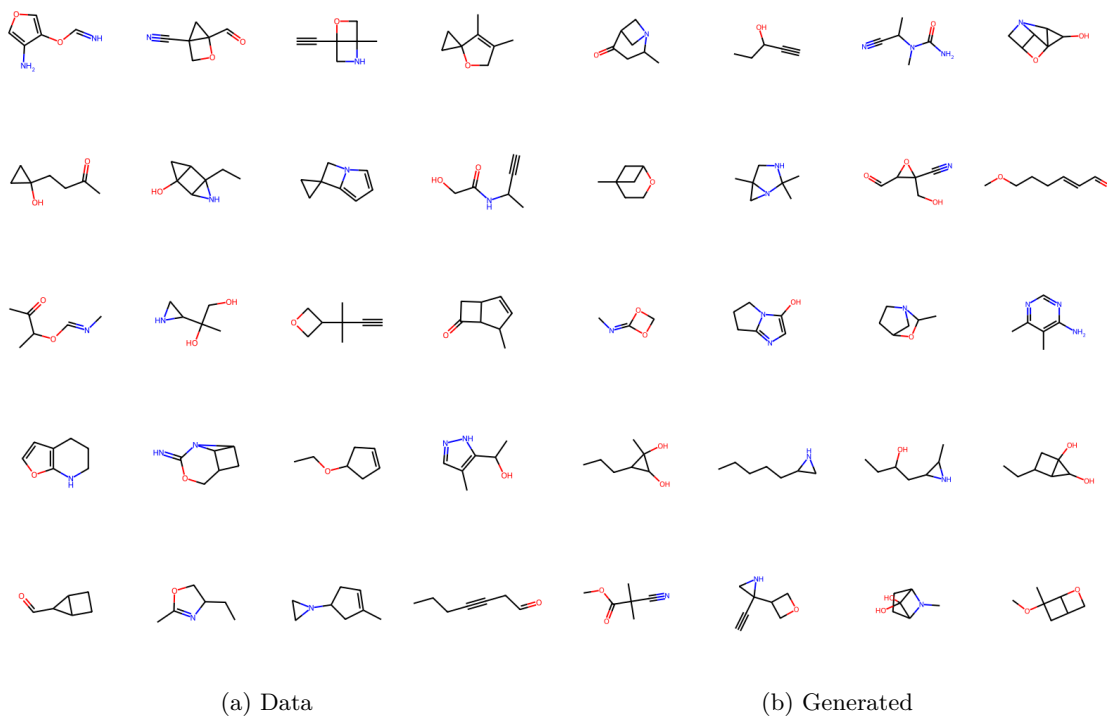


Figure 9: Example of graphs from the Qm9 dataset and from generated samples.



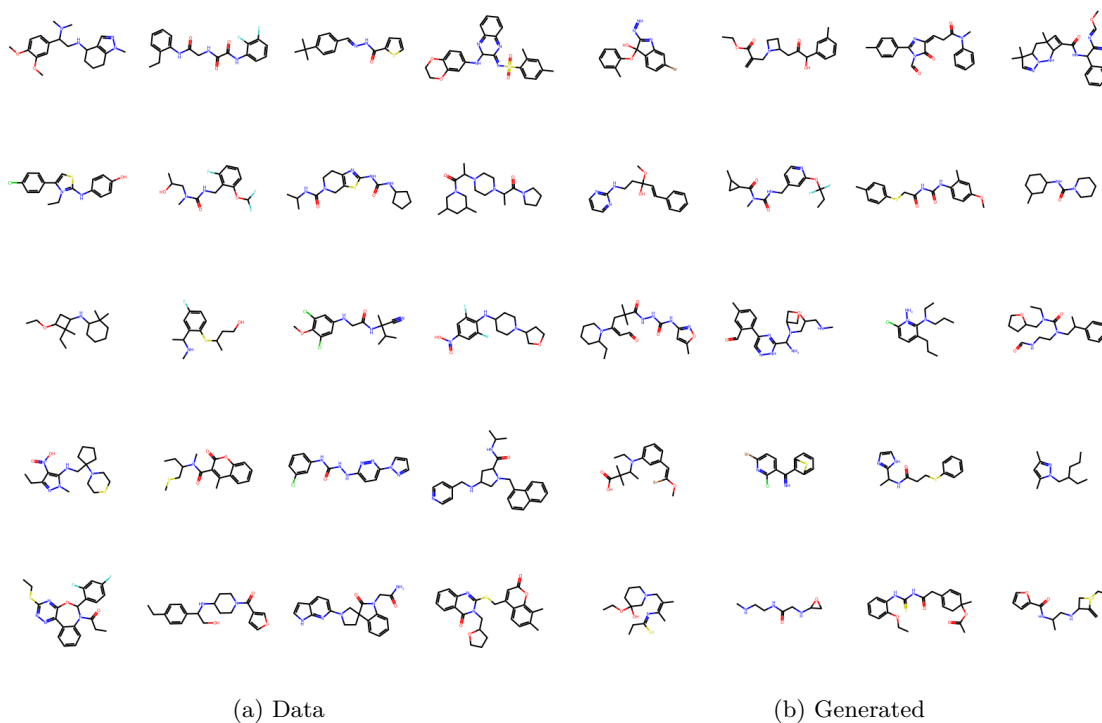


Figure 10: Example of graphs from the Zinc250K dataset and from generated samples.

### C.1 Additional experimental results

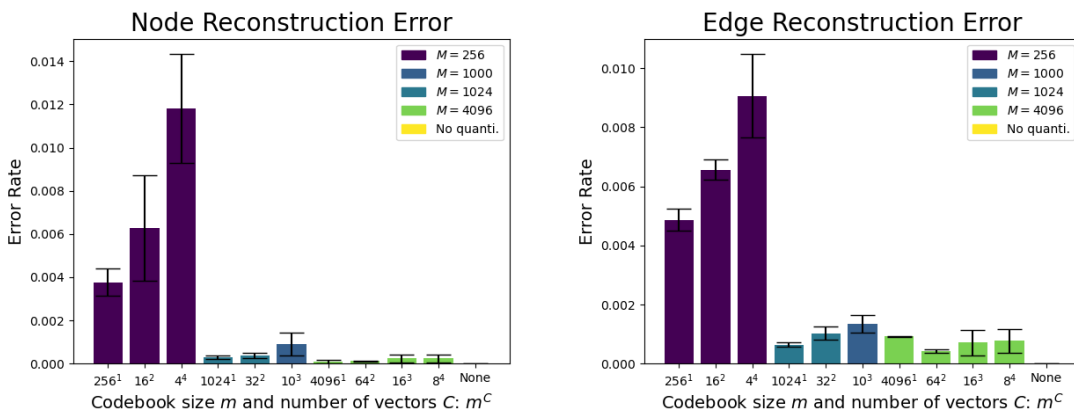


Figure 11: Effect of the codebook size and the partitioning on node (left) and edge (right) reconstruction errors. We report the best error rates averaged over 3 runs. The black lines indicate the standard deviations.

## D Feature augmentation

We use 4 types of feature augmentations:  $p$ -path information, spectral information, cycles information, and random features.

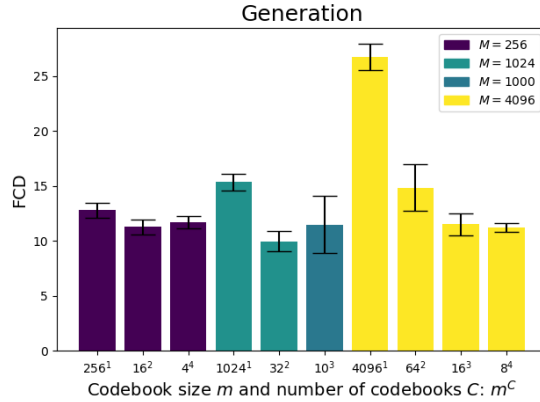


Figure 12: We report the average of the best reconstruction loss over 3 runs. The black lines indicate the standard deviations.

### D.1 Paths feature

The  $p$ -paths information is the number of paths of length  $p$  connecting to nodes. We remind that path is a walk in which all edges and vertices are distinct. However, we allow the first and last vertices to be the same (cycles). We only compute the paths up to  $p = 3$ . We use the following formulas, where  $A$  is the adjacency matrix,  $D$  is the diagonal matrix of degrees and  $I$  is the identity matrix. We assume that the original graph is connected.

$$P_1 = A$$

$$P_2 = A^2 - D$$

$$P_3 = A^3 - AD - (D - I)A$$

We incorporate this information as a vector  $e_{i,j}^p$  of edge attributes  $e_{i,j}^p = [p_{1(i,j)}, p_{2(i,j)}, p_{3(i,j)}]^T$ . We adapt the definition of the neighborhood to include all nodes that are reachable with one of the paths. Similarly, we incorporate the  $p$ -degrees  $p_{j,i}$  ( $p_j = P_j \mathbf{1}$ ) as a vector of node attributes.

### D.2 Spectral feature

The spectral features that we use are the  $k$  eigenvector associated with the  $k$  smallest eigenvalue of the Laplacian  $L$ , which is defined as  $L = D - A$ . Each value in the eigenvectors are associated with one node. By taking the  $k$  first eigenvector, we create a vector of size  $k$  of synthetic node attributed.

### D.3 Cycles feature

The  $c$ -cycle information consists of the number of cycle of size  $c$  a node is part of. As in Digress Vignac et al. (2023), we incorporate the information of  $c \in \{3, 4, 5\}$ . The formulas for the computation are given in the Appendix of Vignac et al. (2023).

### D.4 Random feature

The random features are simply random value sampled from a known distribution. We used the standard Gaussian distribution and a vector size of 4.

### D.5 Examples of indistinguishable graph substructures

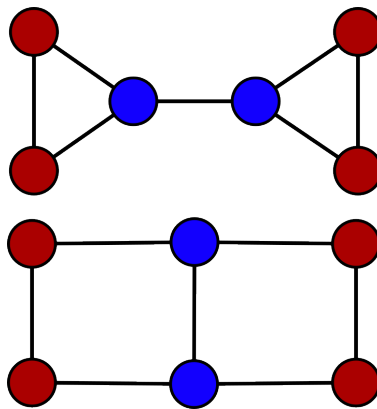


Figure 13: Assuming these two graphs are unannotated, any standard MPNN yields the same node features for all the red nodes as well as for all the blues nodes. It is an example, where MPNN cannot distinguish simple substructures as triangles and squares. However, any of the above methods yield synthetic features that theoretically allow MPNN to distinguish the nodes in the upper graph from the ones in lower graph.